Extended x-ray-absorption fine-structure and x-ray-absorption near-edge-structure studies of glassy $Ni_{66}B_{33}$: A multishell modeling of the Ni-Ni distribution

Joe Wong and Howard H. Liebermann*
General Electric Company, Corporate Research and Development Center, P.O. Box 8, Schenectady, New York 12301
(Received 1 August 1983)

Amorphous $Ni_{66}B_{33}$ is a novel metallic glass in that the metalloid content is much higher than those of conventional transition-metal—metalloid systems. More interestingly, this amorphous material crystallizes homogeneously into a single Ni_2B phase of known crystal structure (that of Al_2Cu) in which there is only one nonequivalent Ni site. The existence of the $Ni_{66}B_{33}$ composition as a single phase in both the crystalline and glassy states makes it a useful model system for quantitative extended x-ray-absorption fine-structure (EXAFS) investigation of the local atomic environment in metal-metalloid glasses. The local structure of a Ni atom in crystalline Ni_2B consists of four boron atoms at a distance of 2.14 Å, one Ni atom at 2.37 Å, two Ni atoms at 2.42 Å, and two sets of four Ni atoms at 2.63 and 2.70 Å. The Ni_2B crystal was used to model the local structure of Ni in the metallic glass as follows: Crystallographic data (coordination numbers and bond distances) were used as fixed inputs to the Fourier-filtered EXAFS of the crystal to generate an envelope function for B and a set of self-consistent phase shifts for the Ni-B and Ni-Ni pairs. These scattering parameters were then transferred as fixed inputs to the Fourier-filtered EXAFS of the glass phase to extract structural parameters. The fitting of the glass EXAFS was performed systematically using sequentially 1 B + 1 Ni shells, 1 B + 2 Ni shells, 2 B + 1 Ni shells, 1 B + 3 Ni shells, 2 B + 2 Ni shells, and 1 B + 4 Ni shells. It was found that the 1 B + 3 Ni shell combination yields the best fit and physically most meaningful results for the glass. It was also found that the nearest boron shell about a Ni atom in the glass remains very similar to that of the crystal, but there is considerable rearrangement of the outer Ni shells. In the glass, the eleven Ni atoms are now distributed into three subshells with the shortest Ni-Ni distance measurably closer to the central Ni atom. This local rearrangement and closer packing of the Ni shells were reflected in the local electronic structure of the glassy phase and manifested in changes of the x-ray-absorption near-edge structure spectrum in going from the crystal to the glassy phase. Ge substitution was made to probe the metalloid environment in glassy $Ni_{66}B_{15}Ge_{18}$. The present EXAFS findings are discussed in light of some recent diffraction and NMR results in Ni-B glasses.

I. INTRODUCTION

Glassy metallic alloys formed by splat quenching the corresponding liquids at rates $\sim 10^6$ K/s (Ref. 1) constitute a novel class of amorphous solids. These materials can exhibit high electrical conductivity, ferromagnetism, and superconductivity, which are not found in conventional inorganic and organic polymeric glasses. Other interesting properties include high ductility in bending, corrosion resistance, and good soft magnetic properties. These properties,[2] not found in the crystalline counterparts, have aroused considerable technological[3] as well as scientific[4] interest in recent years. It has not been established that certain groups of related alloys exist for which this glassy phase is relatively stable. Glass-forming metallic alloys may broadly be classified into two types: (I) transition metal plus metalloid and (II) metal plus another metal. Type-I metallic glasses are exemplified by the well-known $Au_{80}Si_{20}$, $Pd_{80}Si_{20}$, and $Ni_{80}P_{20}$ glasses are more recently the $(Fe,Ni)_{80}(P,B)_{20}$ ferromagnetic glasses first produced at Allied Corporation. Type-II metallic glasses may be generically represented by T'-T'', R-T'', and M'-M'', where T' is an early transition metal such as Ti,Zr,Nb; T'' is a late transition metal such as Fe,Co,Ni,Cu; R is a rare-earth metal such as Gd,Tb,Dy; and M'-M'' are simple metal binaries such as $Be_{70}Al_{30}$ (Ref. 5) and $Mg_{70}Zn_{30}$ (Ref. 6).

The formation of transition metal-metalloid ($T_{100-x}M_x$) glassy alloys by rapid quenching from the melt is usually confined to a limited composition range of about $15 \leq x \leq 25$. Glass formation in this composition range is now known to be facilitated by the presence of a deep eutectic.[7] In contrast with type-I alloys, the glass-forming composition range of T'-T'' alloys occurs in the middle of the binary and is usually wider than for type-I alloys. In the case of splat-quenched $Nb_{100-x}Ni_x$, x ranges from 40 to 70 (Ref. 8) and can be expanded to 30—85 at.% Ni by vapor quenching.[9] More detailed listings of both types of glass-forming metallic systems have been given by Takayama[10] and Donald and Davies.[11] The structure of such T-M glasses has been postulated by Polk[12] to be comprised of a dense random packing of hard spheres (DRPHS), simulating the metal atoms, which form a bulk matrix built up from an ensemble of various Bernal polyhedra.[13] The metalloid atoms are said to be situated at the larger holes of eightfold- or ninefold-coordination in the metal atom polyhedral network. Furthermore, Polk has estimated that all the holes avail-

able would be filled with metalloid atoms at the atomic ratio $[T]$:$[M]$ of 80:20. As is well documented in the literature, the glass-forming composition range for a wide variety of T-M alloys lies in the vicinity $15 \lesssim x \lesssim 25$, near the anticipated 20-at.% metalloid content.[10,11] This simple model further postulates that there are no metalloid-metalloid nearest neighbors and that the metal-metalloid distance will be smaller than the sum of the atomic radii of the constituent atoms. Early diffraction[14] and extended x-ray-absorption fine-structure[15] (EXAFS) results obtained for $T_{80}M_{20}$-type glasses generally substantiated the Polk model, but there are quantitative differences.[16–20]

Glassy alloys of the type T-M substantially away from the 80:20 atomic ratio have been prepared. Inoue *et al.*[21] have reported on metallic glasses in the Ni-B and Co-B systems containing 33—43 and 35—41 at.% B, respectively. These high-metalloid systems pose the following interesting questions relevant to the applicability of the Polk model: (i) Where do the additional metalloid atoms reside in the DRPHS structure at concentration $x > 25$ (at.%)? (ii) Do they go into other Bernal holes of lower coordination numbers? (iii) Do they modify the basic dense random packing of the metal matrix? or (iv) do they go into the structure as nearest neighbor, violating the metalloid-metalloid avoidance postulated for the 80:20 system? Furthermore, it is instructive to compare and contrast the local structure between these high-metalloid content glasses and that of the metal-metal glasses such as those in the $Zr_{100-x}Ni_x$ system,[22] which also has a wide composition range of glass formation in the middle of the binary for $x = 30$—70.

An experimental advantage of high boron-content metallic glasses like those in the Ni-B system is that the glass at the composition $Ni_{66}B_{33}$ crystallizes homogenously upon annealing into a single Ni_2B phase[23] of known crystal structure—that of Al_2Cu ($C16$) -type structure.[24] The existence of the $Ni_{66}B_{33}$ composition in both the crystalline and glassy phases makes it an attractive experimental system for quantitative EXAFS investigation of the local atomic environment in metal-metalloid glasses. This is because the crystal can be used as reference material to generate self-consistent phase shift and/or backscattering amplitude functions which in turn can be transferred for evaluating bond distances and coordination numbers in the glassy phase. Such an advantage, however, does not occur in the $T_{80}M_{20}$ glasses, since their crystallization yields a mixture of pure T, T_3M, and other T-M phases.[25–28] Another advantage, from an EXAFS point of view, is that it is possible to substitute Ge for B in these high boron-content glasses to concentrations in such a way that Ge can become the majority metalloid component[23] (e.g., $Ni_{66}Ge_{18}B_{15}$). The metalloid environment can now be probed by measuring and analyzing the EXAFS above the Ge K edge at 11.1 keV. This energy is readily accessible at Stanford Synchrotron Radiation Laboratory (SSRL).

A number of diffraction studies on Ni-B glasses have been reported in the literature covering compositions at $Ni_{81}B_{19}$ (Refs. 19 and 29), $Ni_{71}B_{29}$ (Ref. 30), and $Ni_{66}B_{34}$.[29,30] The neutron diffraction investigation using the isotopic substitution method on both ^{62}Ni- and ^{11}B-enriched $Ni_{81}B_{19}$ glasses by Lamparter *et al.*[30] to determine the Ni-Ni, Ni-B, and B-B partial structural factors is by far the most detailed and elucidative. Most recently Panissod *et al.*[31] have reported a comparative study the B environments in glassy alloys and nickel boride compounds in the $Ni_{100-x}B_x$ system ($x = 18.5$—40) using ^{11}B NMR. In the present paper we report on detailed local structural investigation in glassy $Ni_{66}B_{33}$ using crystalline Ni_2B to model the Ni environment in the glass in our EXAFS analysis. Ge substituted into the binary glass is used to probe the metalloid environment. The x-ray-absorption near-edge structure, the so-called XANES, at both the Ni and Ge K edges was used to probe the metal-metalloid interactions. Finally, our x-ray absorption results will be compared with the available diffraction and NMR results.

II. EXPERIMENTAL

Master alloys of compositions $Ni_{66}B_{33}$, and $Ni_{66}B_{33-y}Ge_y$ ($y = 6, 12, 18$) were premelted using high-purity Ni (99.98%), B (99.99%), and Ge (99.9999%). Details of their preparation and characterization have been given earlier.[23] Rapidly quenched glassy ribbons of the alloys were fabricated by chill block melt-spinning in air.[32] Samples thus formed had a cross section of $\sim 10\,\mu$m thick by ~ 1 mm wide. This thickness corresponds to about 2 absorption lengths of Ni in these alloys above its K absorption edge at 8332.8 eV,[33] and was achieved by careful control of the melt-spinning apparatus configuration and process conditions.[32,34] With this thickness, the as-cast ribbons can be used directly for transmission EXAFS measurements without any mechanical thinning after checking for the amorphous nature by the bend ductility testing and x-ray diffraction. EXAFS specimens were then prepared by carefully laying four pieces of 5-cm-long ribbon strips side by side on an aluminum sample holder so that the synchrotron x-ray beam totally permeated the specimen. The sample holder was mounted onto the cold finger of a double-wall cryostat cooled with liquid nitrogen.

Initially three specimens of crystalline Ni_2B were obtained: (a) master $Ni_{66}B_{33}$ alloy from our own in-house melting in powder form; (b) ribbon samples crystallized by annealing the $Ni_{66}B_{33}$ glassy ribbons at 550 °C for 2 h in purified Ar [T_g of glassy $Ni_{66}B_{33} = 379$ °C (Ref. 23)], and (c) commercial "Ni_2B" powder from Cerac, Inc. X-ray diffraction analysis showed that both (a) and (b) consist of a pure Ni_2B phase[35] while (c) consisted of Ni_2B as a major phase with Ni_3B as a minor phase. Only specimen (b) was used for EXAFS measurements since it was directly crystallized from the glassy phase of the same material and was in the ribbon form. Specimen (a) could have been used, but at a risk of having pin-hole and thickness nonuniformity in the spectral specimen, both of which causes errors in the transmitted intensity, and hence inaccuracy in amplitude functions.

Transmission XANES and EXAFS measurements were made at room temperature with the EXAFS I-5 spectrometer at SSRL during a parasitic run of SPEAR (Stanford

Positron Electron Accelerator Ring) at an electron energy of 2.4 GeV and storage ring injection current ~15 mA. The synchrotron x-ray beam from SPEAR was monochromatized with a channel-cut Si(220) crystal which yielded an energy resolution of ~0.7 eV for the Ni K edge at 8332.8 eV and ~1 eV for the Ge K edge at 11 103.1 eV.[33] A Ni-metal foil and Ge powder (−400 mesh, then further jet-milled) film dispersed in Duco® cement were used to calibrate the spectrometer. The Berkeley software[36] was used to collect the XANES and EXAFS data. Since the measured disorder σ^2_{total} is a sum contribution of thermal σ^2_{th} and structural σ^2_s, disorder, EXAFS scans of liquid-nitrogen-cooled samples (~90 K) were also recorded in order to minimize thermal broadening and to bring out the structural effects in which we are interested.

III. RESULTS AND DATA REDUCTION

The Ni K edge EXAFS spectra at ~90 K for glassy $Ni_{66}B_{33}$ and Ni_2B crystallized from the glass are shown in part (a) of Figs. 1 and 2, respectively. Since the K edge of boron (188 eV) is too low in energy to be measured with the x-ray radiation emerges from the Be window (which

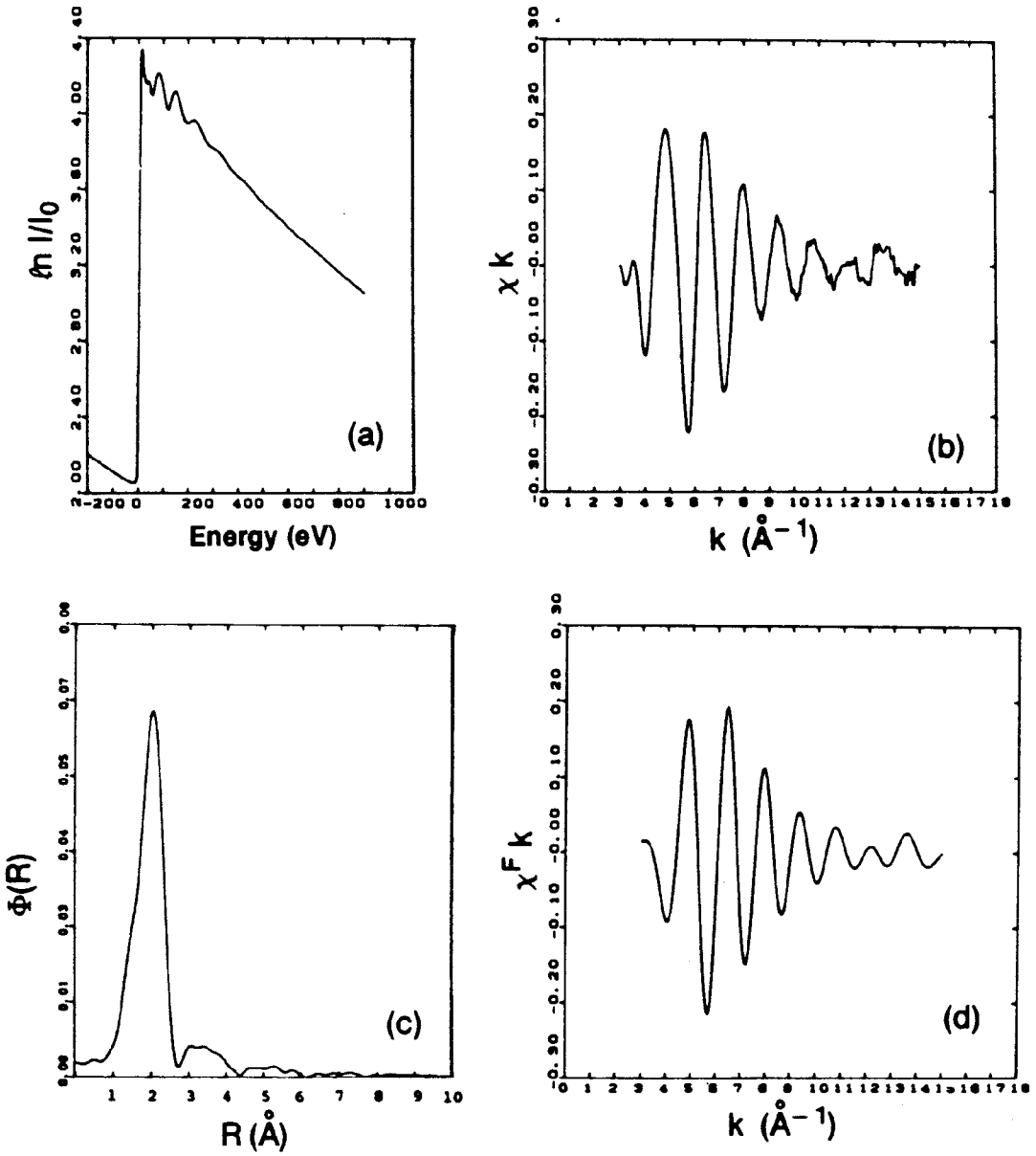

FIG. 1. (a) Experimental scan of Ni K-edge XANES and EXAFS in $Ni_{66}B_{33}$ glass at ~90 K, the energy scale is with respect to the Ni K-edge energy (8332.8 eV) taken as zero. (b) Normalized EXAFS as χk vs k. (c) Fourier transform of (b). (d) Inverse transform of (c) in the region 1–2.8 Å. The $\Phi(R)$ scale in (c) has been multiplied by 10.

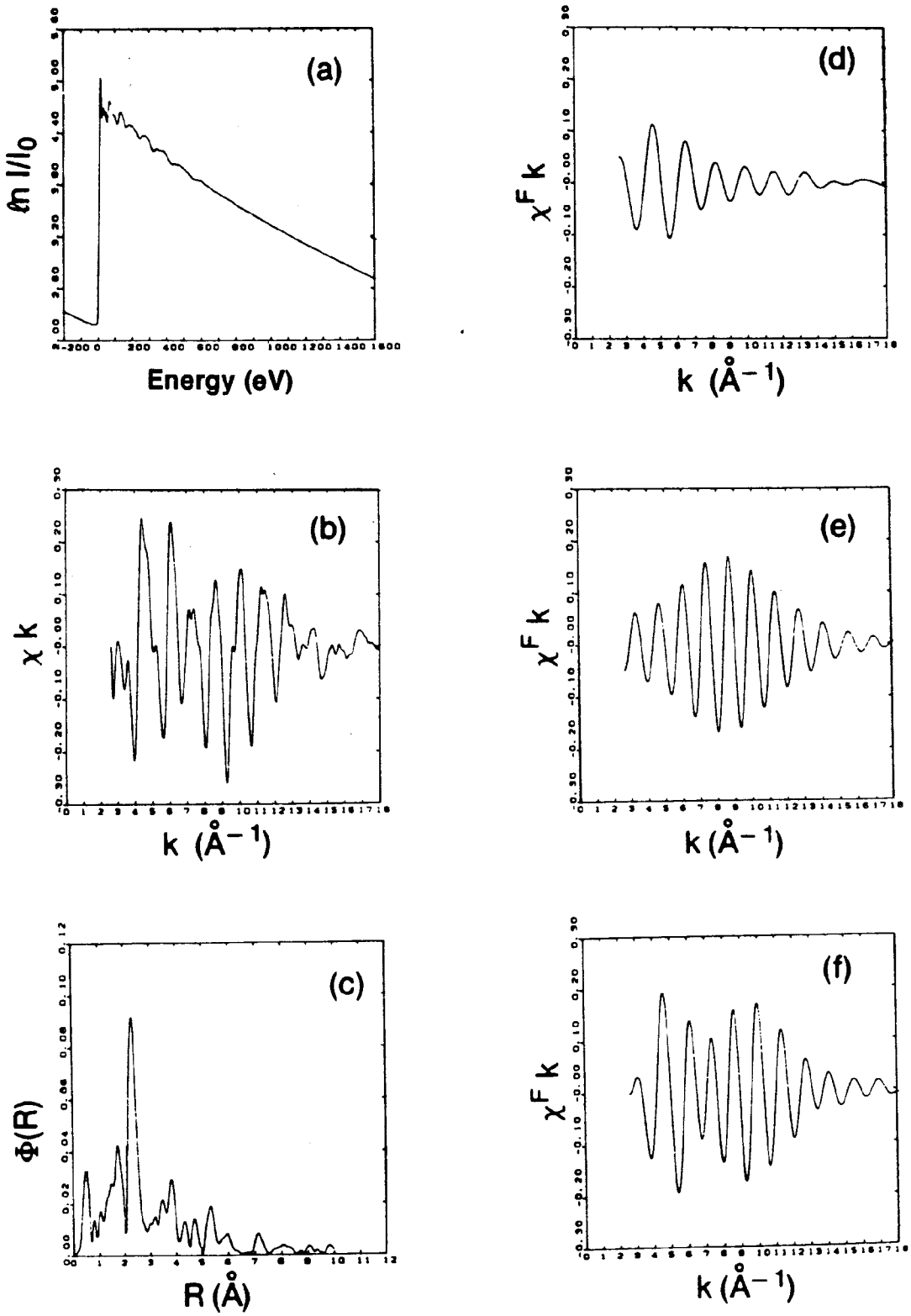

FIG. 2. (a) Experimental scan of Ni K-edge XANES and EXAFS in crystalline Ni_2B at ~90 K. (b) Normalized EXAFS. (c) Fourier transform of (b). (d) Inverse transform of (c) in the region 1–2 Å. (e) Inverse transform of (c) in the region 2–3 Å. (f) Inverse transform of (c) in the region 1–3 Å. The $\Phi(R)$ scale in (c) has been multiplied by 10.

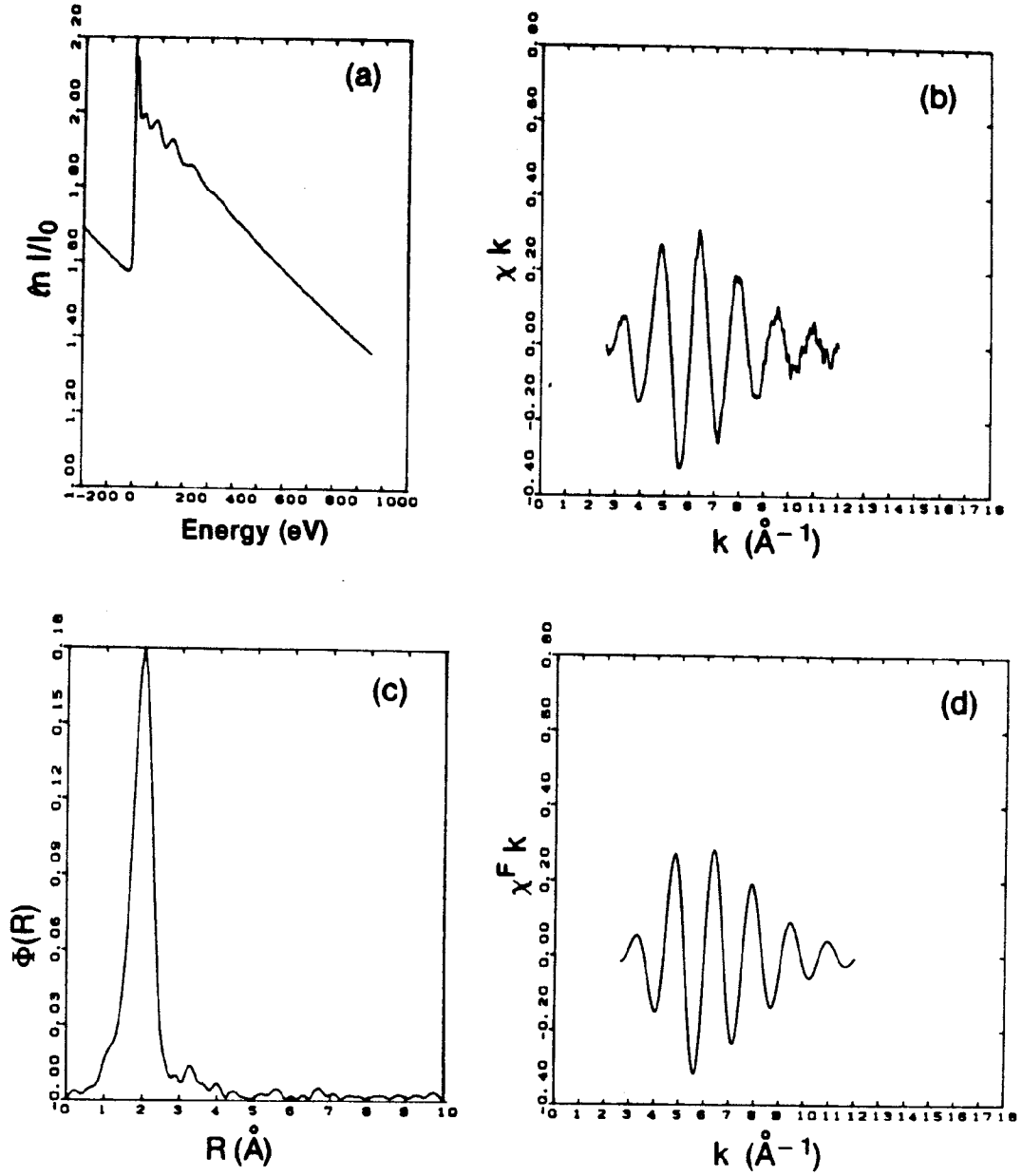

FIG. 3. (a) Experimental scan of Ge K edge XANES and EXAFS in $Ni_{66}B_{15}GE_{18}$ glass at ~90 K, the energy scale is with respect to the Ge K-edge energy (11 103 eV) taken as zero. (b) Normalized EXAFS. (c) Fourier transform of (b). (d) Inverse transform of (c) in the region 0.5—2.8 Å. The $\Phi(R)$ scale in (c) has been multiplied by 10.

absorbed most of the radiation below 2.5 keV) of the EXAFS I-5 spectrometer, Ge substitution was made and used as a probe for the metalloid environment in the Ni-B glass. Ge was progressively added in glassy $Ni_{66}B_{33-y}Ge_y$ ($y = 6, 12, 18$) until it became the major metalloid constituent. The low-temperature Ge K edge spectrum for $Ni_{66}B_{15}Ge_{18}$ is shown in Fig. 3(a). This EXAFS spectrum after normalization (see below) was shown to be identical to those with $y = 6$ and 12. Room-temperature EXAFS spectra of the same samples were also recorded, and exhibited in each case identical jump at the absorption edge as expected since this is a direct measure of sample thickness. However, the magnitude of the EXAFS oscillations above ~30 eV decreases, which indicates thermal broadening.

Data reduction followed a standard procedure[37–40] of correcting for spectrometer shift, deglitching, pre-edge and post-edge background removal, edge normalization, extraction of the EXAFS signal $\chi(k)$, Fourier transform of $\chi(k)$, and inverse transform to isolate the EXAFS contribution from a selected region in real space. The pre-edge background in the range −200 to −20 eV is ob-

tained by a linear regression analysis of the first ten raw data points. The post-edge background above 30 eV in the EXAFS region was generated analytically using a series of cubic splines[41] of equal segments. The ends of each segment are so connected that the derivatives are continuous across the ends. Five such splines were found adequate. When the number of segments is too small the background is not separated well enough; when the number is too large the background follows the EXAFS oscillations, especially at low energy, and "robs" its intensity.[39] The energy scale was then converted to the k scale using

$$k=(1/\hbar)[2m(E-E_0)]^{1/2}=[0.263(E-E_0)]^{1/2}$$

where E_0 is the energy threshold of the absorption edge.[33] The normalized EXAFS $\chi(k)$ at energies above ~ 30 eV was obtained by subtracting the smooth post-edge background $\mu_0(k)$ from the measured absorption $\mu(k)$ and dividing by the step jump S at the absorption edge with the McMaster correction[42] $M(k)$ as a function of energy:

$$\chi(k)=\frac{\mu(k)-\mu_0(k)}{SM(k)} \tag{1}$$

The Fourier transform of $\chi(k)$ yields a radial structure function $\Phi(R)$ in real space:

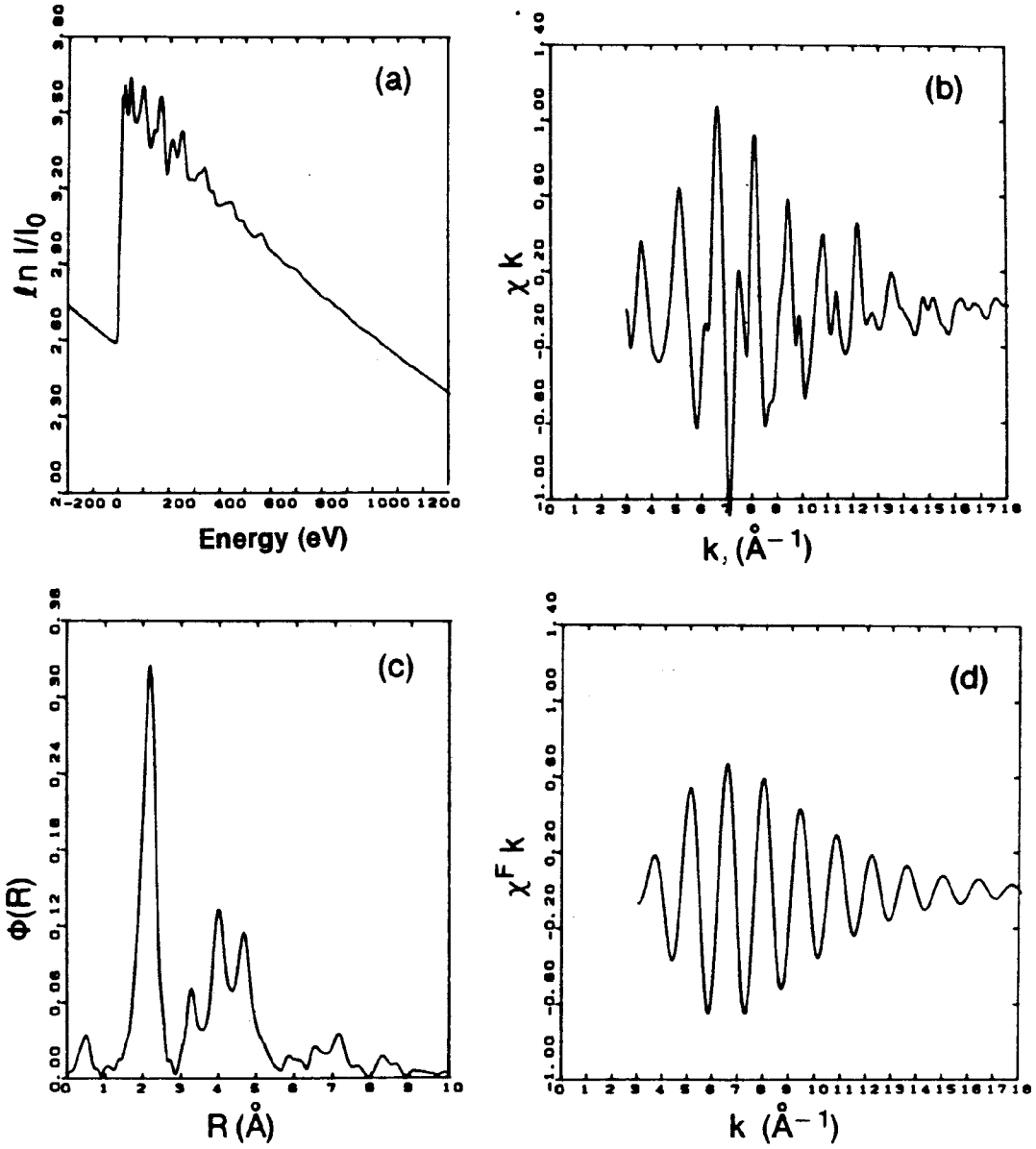

FIG. 4. (a) Experimental scan of Ni K-edge XANES and EXAFS in pure Ni metal at ~ 90 K. (b) Normalized EXAFS. (c) Fourier transform of (b). (d) Inverse transform of the first shell in (c) in the region 1–2.8 Å. The $\Phi(R)$ scale in (c) has been multiplied by 10.

$$\Phi(R)=(2\pi)^{-1/2}\int_{k_{\min}}^{k_{\max}} W(k)k^n\chi(k)\exp(2ikR)dk \ , \quad (2)$$

where $W(k)$ is a Hanning function defined as

$$W(k)=\tfrac{1}{2}\left[1-\cos 2\pi\left[\frac{k-k_{\min}}{k_{\max}-k_{\min}}\right]\right] \quad (3)$$

and was applied to the first and last 1% of the usable EXAFS data defined by $k_{\min}$ and $k_{\max}$ and $n=1$, 2, or 3 to weigh the data in $\vec{k}$ space.[38]

In Fig. 1(b) the normalized Ni EXAFS for glassy $Ni_{66}B_{33}$ is plotted as χk vs k. The Fourier transform of this signal [Fig. 1(c)] yields a broad radial peak at ~ 2 Å, which is asymmetric on the low-R side. Inverse transform of this radial structure peak in the region 1–2.8 Å yields a filtered $\chi^F k$ signal in $\vec{k}$ space [Fig. 1(d)], which was used to simulate the local structure of Ni in the glass (see below).

In Fig. 2(b) the normalized Ni EXAFS for crystalline Ni_2B is plotted also as χk vs k. The Fourier transform of

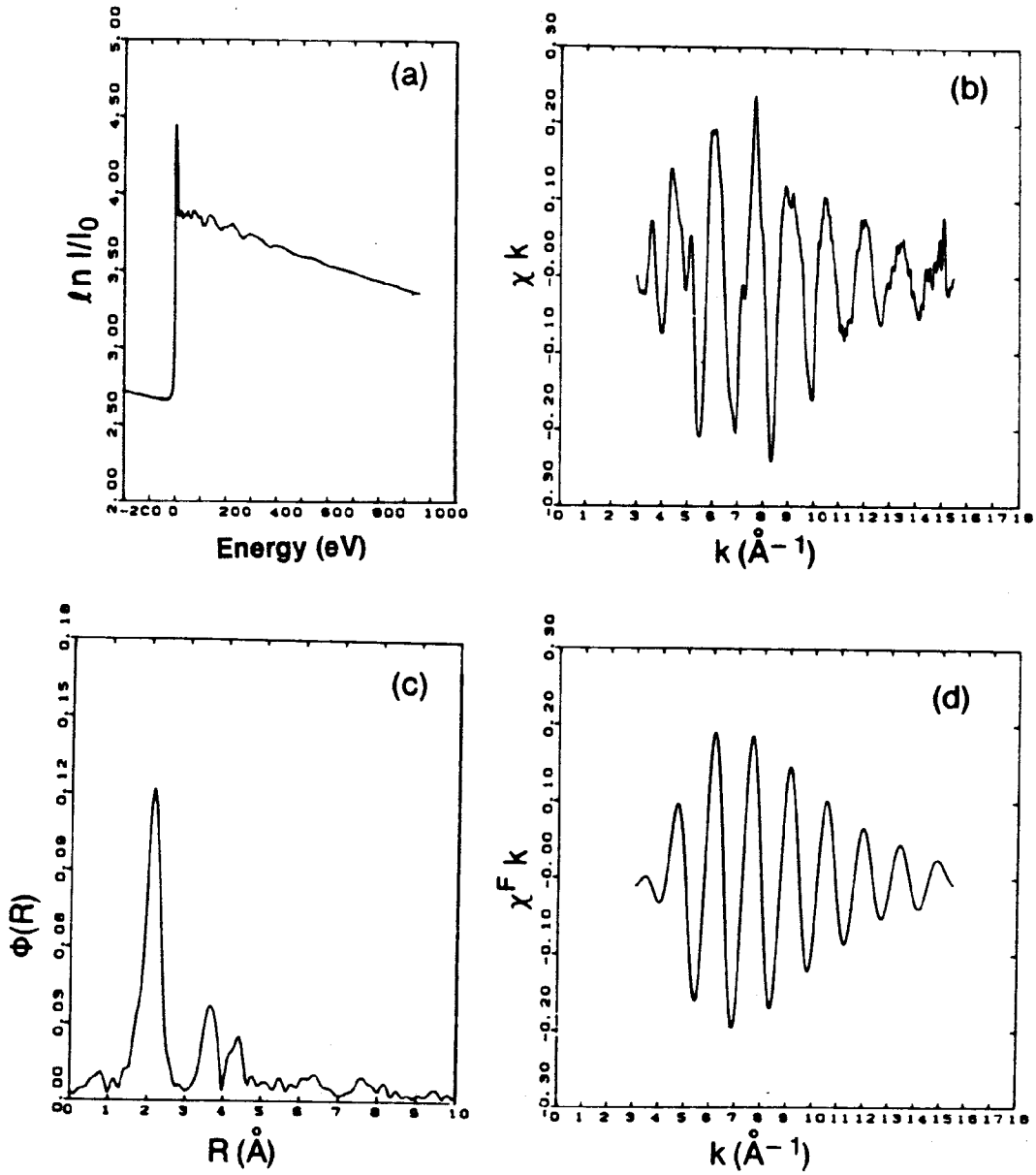

FIG. 5. (a) Experimental scan of Ge K-edge XANES and EXAFS in pure Ge at room temperature. (b) Normalized EXAFS. (c) Fourier transform of (b). (d) Inverse transform of the first shell in (c) in the region 1–3 Å. The $\Phi(R)$ scale in (c) has been multiplied by 10.

this signal [Fig. 2(c)] yielded a number of distinct radial peaks to at least 6 Å from the Ni center. The spikes below 1 Å are artifacts of the transform and have no structural significance. The two peaks in the range 1–3 Å are of direct relevance in modeling the short-range order environment of Ni in the corresponding glass. An inverse transform of the first structural peak in the range 1–2 Å yields a filtered $\chi^F k$ signal [Fig. 2(d)] which has a monotonic decreasing envelope typical of a low-Z element like boron.[43] In the region 2–3 Å an inverse transform of the second structure peak in Fig. 2(c) yields a filtered $\chi^F k$ signal [Fig. 2(e)] which has a maximum in the envelope typical of a $3d$ element like nickel. Finally, an inverse transform of the combined two peaks in the region 1–3 Å yields a filtered $\chi^F k$ signal [Fig. 2(f)] which is a superimposition of those in Fig. 2(d) and 2(e), and consists of an initial decreasing signal at low k and a maximum in the region of $k \sim 9.5$ Å^{-1}.

In Fig. 3(b) the normalized Ge EXAFS for glassy $Ni_{66}B_{15}Ge_{18}$ is plotted as χk vs k. Fourier transforms of this signal [Fig. 3(c)] yield a single, symmetric peak in the radial structure function. This indicates that the nearest-neighbor environment of Ge is quite well ordered in the glass. The inverse transform [Fig. 3(d)] of this peak in the region 0.5–2.8 Å yields a filtered $\chi^F k$ signal that is nearly identical (except for the high-frequency noise) to the total experimental signal, implying that the observed EXAFS intensity comes entirely from within ~3 Å of the absorbing Ge atom in the glass. Glasses containing 6 and 12 at.% Ge gave identical Ge EXAFS when normalized.

Finally, the K edge EXAFS spectra of pure Ni and Ge, their normalized EXAFS, Fourier transforms, and inverse transforms of the first structural peak in the regions 1–2.8 Å and 1–3 Å are shown in Figs. 4(a)–4(d) and Figs. 5(a)–5(d), respectively. The Ni spectrum was taken at ~90 K and the Ge spectrum was obtained at room temperature. As discussed in the next section, the first shell inverse transform of these two materials was used to extract a set of self-consistent phase shifts and envelope functions for the Ni-Ni and Ge-Ge atom pairs which are used as input scattering parameters in simulating the structure of $Ni_{66}B_{33}$ and $Ni_{66}B_{15}Ge_{18}$ glasses by curve fitting to the experimental data. Also, the near-edge absorption spectra in the range ±60 eV of both Ni and Ge were used to evaluate the local electronic interaction (chemical bonding) of the metal and metalloid atoms in the glasses.

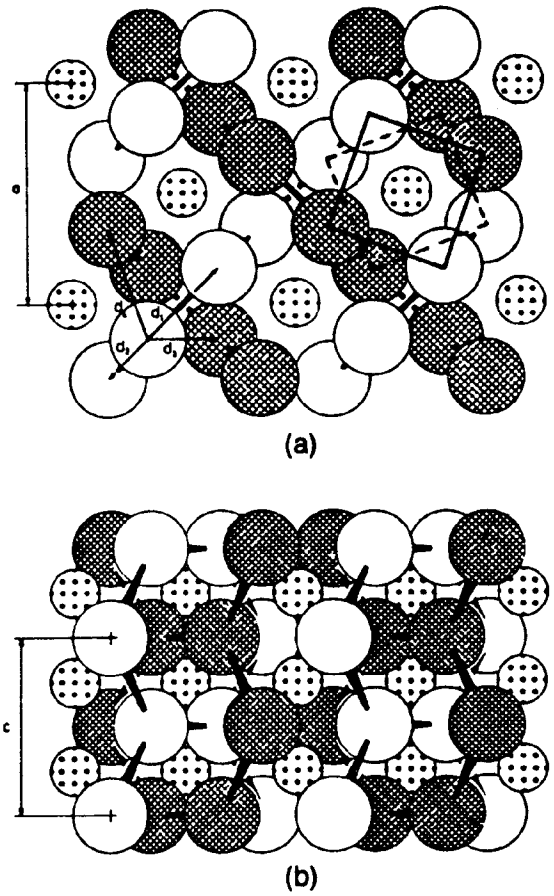

FIG. 6. (a) (110) and (b) (001) projections of the idealized $C16$-type structure for Ni_2B showing the packing and local coordination geometry of Ni and B. The Ni atoms lying the (110) hexagonal network are shaded to distinguish them from Ni atoms in the $(1\bar{1}0)$ hexagon network. The dotted circles denote B atoms. In (a) the solid and dotted squares define the top and bottom faces of an Archimedean square antiprism of Ni atoms around a given B atom. (After Havinga *et al.*, Ref. 24.)

IV. DISCUSSION

A. Structure of crystalline Ni_2B

Ni_2B belongs to the Al_2Cu ($C16$) -type structure[24]: body-centered tetragonal, space group D_{4h}^{18} ($I4/mcm$), and $Z=4$ Ni_2B units per cell. The eight Ni atoms are in C_{2v} sites and four B atoms are in D_4 sites. Each B atom is coordinated with eight Ni atoms situated at the corners of an Archimedian square antiprism [see Fig. 6(a)] and has two noncontracting B atoms as a distance of $r_{B\text{-}B}=c/2=2.12$ Å, which is larger than twice the radius of the B atom of 1.86 Å [see Fig. 6(b); c is the c parameter of the tetragonal unit cell]. The local of each Ni atom consists of a shell of four nearest B neighbors at 2.14 Å, which give rise to the first radial peak in the region 1–2 Å of the Fourier transform in Fig. 2(c). The Ni atom is also surrounded by $1+2+4+4=11$ Ni atoms at 2.37 Å (d_1), 2.43 Å (d_2), 2.70 Å (d_3), and 2.63 Å (d_4) [see Fig. 6(a)]. This set of Ni neighbors combine to give the second radial peak in the region 2–3 Å of the Fourier transform [Fig. 2(c)]. Of significance in this structure is the short Ni-Ni distances, d_1 and d_2, which are shorter than the Ni-Ni distance in fcc Ni metal. According to the description of Hagg,[44] the Ni atoms form two sets of mutual orthogonal planes with a dense packing of hexagon parallel to (110) and$(1\bar{1}0)$, respectively. The hexagons of the different sets are fully interlocking as depicted in Fig. 6(b). The B atoms are situated as linear chains in the channels parallel to the c axis, which are formed by this interlocking honeycomb structure.

B. Experimentally determined Ni-B, Ni-Ni, and Ge-Ge phase shifts and B, Ni Ge amplitude functions

In the single-scattering approximation,[37,38] the observed EXAFS $\chi(k)$ may be described by

$$\chi(k)=\frac{-1}{k}\sum_j A_j \sin[2r_j k+\phi_j(k)] , \tag{4}$$

having oscillatory terms with frequencies $[2r_j k+\phi_j(k)]$, and amplitude terms A_j given by

$$A_j=\frac{N_j}{r_j^2}f_j(\pi,k)\exp\left[\frac{-2r_j}{\lambda}\right]\exp(-2\sigma_j^2 k^2) . \tag{5}$$

The parameters on the right-hand side of Eqs. (4) and (5) may be classified as (a) scattering parameters, which include phase shift $\phi_j(k)$, backscattering amplitude $f_j(\pi,k)$, and mean free path λ, and (b) structural parameters, which include coordination number N_j, bond distance r_j, and Debye-Waller factor σ_j. The summation is over all coordination shells j participating in the EXAFS event. In a model system such as Ni_2B for which N_j and r_j are known, EXAFS may be used to generate a set of self-consistent scattering parameters; this information can then be applied to an unknown system of similar chemical nature, which in this case is the glass of the same composition, to determine structural parameters.

A least-squares procedure[45] is set up to minimize the variance S, where

$$S=\sum_i^n (\chi_i^F-\chi_i)^2 . \tag{6}$$

Here χ_i^F are the Fourier-filtered experimental data and χ_i is the analytical expression given in Eq. (4) which describes χ_i^F for n data points. Since $\chi(k)$ is not a linear function of the various parameters, a Taylor-series expansion is used which expresses $\chi(k)$ in terms of approximate parameter values P_j and parameter adjustments $\Delta P_j=P_j-P_j'$. When the least-squares condition is applied, a set of simultaneous equations is obtained in terms of ΔP_j rather than P_j. The equations are solved for the adjustment ΔP_j, and the parameters were adjusted by ΔP_j to give a new set of estimates. The procedure was then reiterated with a new estimate P_j' and so on until the new solution differed from the last by less than a desired value, which is usually 1%.

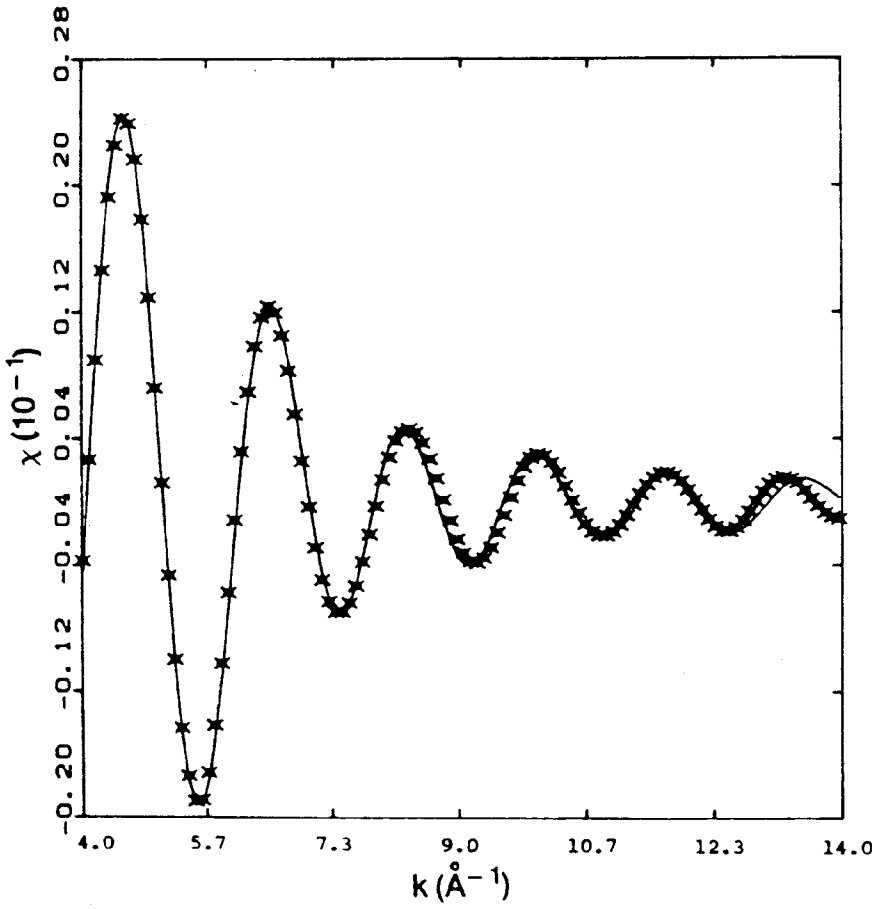

FIG. 7. Experimental (line) and simulated (points) EXAFS from the four B atoms in the region 1–2 Å about the central absorbing Ni atom in crystalline Ni_2B at ~90 K.

1. Determination of Ni-B phase shift and B envelope function

From the Ni EXAFS data, it is evident that the first radial peak in the region 1–2 Å of the Fourier transform for Ni_2B, shown in Fig. 2(c), corresponds to the shell of four B atoms about the absorbing Ni atom in the Ni_2B crystal structure. The inverse transform [Fig. 2(d)] of this peak indeed shows an experimental envelope characteristic of a low-Z backscattering atom, i.e., B. To obtain self-consistent phase shift for the Ni-B pair, the parametrized values of Lee *et al.*[46] in the form

$$\phi = P_0 + P_1 k + P_2 k^2 + P_2/k^3 \tag{7}$$

were used as initial input. The envelope function $f_B(\pi,k)\exp(-2\gamma_j/\lambda)$ for B was obtained empirically from the filtered EXAFS itself [Fig. 2(d)] and was fixed in the simulation. $\Delta E_0[=E_0(\text{theoretical})-E_o(\text{experimental})$ (Ref. 43)] and σ were fixed at zero. $N=4$ and $r=2.14$ Å were used as fixed structural parameters. The simulation was done in χ space to emphasize the backscattering contribution of B at low k. The results are shown in Fig. 7, where the curve denotes the Fourier-filtered spectrum and the points denote the simulated spectrum. The phase parameters and the input values of N and r are given in Table I. The simulation was fitted with a standard deviation of 2.8% of the maximum amplitude of the experimental χ^F function.

2. Determination of Ni-Ni phase shifts and Ni envelope function

To generate the phase and envelope function for the Ni-Ni pair, we first performed a self-fitting of the filtered EXAFS [Fig. 4(d)] of the first shell of 12 nearest neighbors in fcc Ni metal with the following fixed inputs: $N=12$, $r=2.492$ Å, $\Delta E_0=0$, and $\sigma^2=0$. The fitting was performed in χk^3 space to weigh the contribution of Ni at high k. The results are shown in Fig. 8, where the curve denotes the filtered experimental EXAFS and the points denote the simulated spectrum. This simulation has a standard deviation of 5% of the maximum amplitude of the experimental $\chi^F k^3$ spectrum. The Ni-Ni phase parameters so obtained (Table I) were then used as initial inputs to simulate the filtered transform [Fig. 2(e)] arising from the four Ni subshells in the region 2–3 Å [Fig. 2(c)] about the central absorbing Ni atom in crystalline Ni_2B.

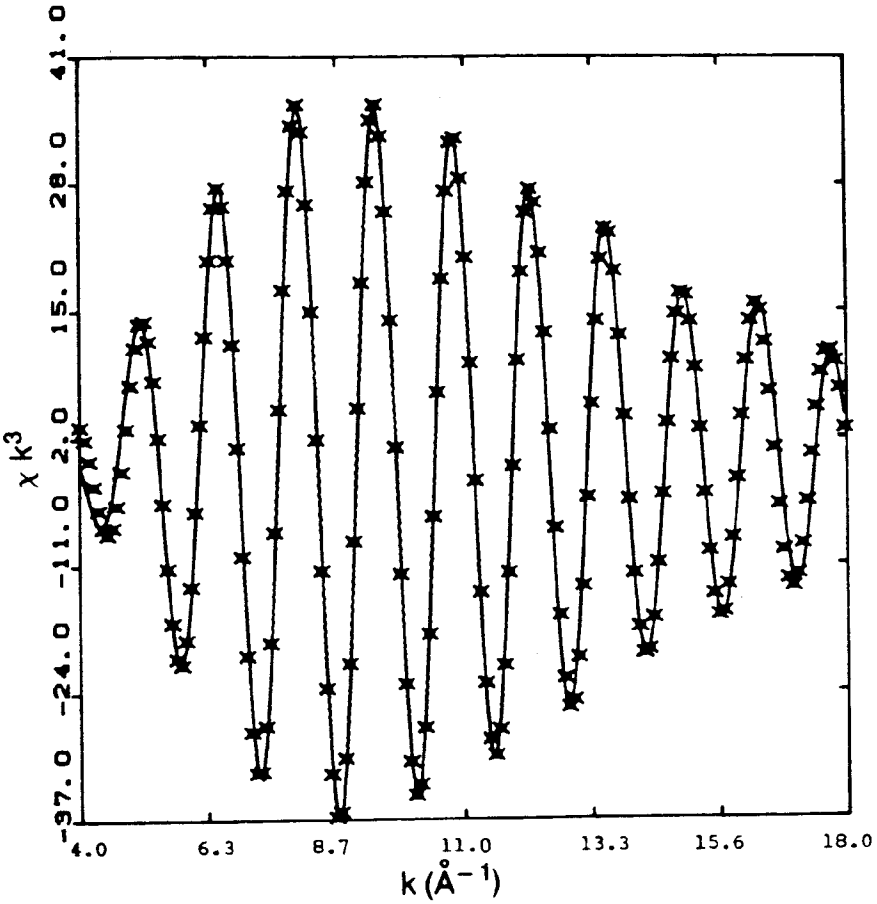

FIG. 8. Experimental (line) and simulated (points) EXAFS of the first shell of 12 neighbors in the region 1–2.8 Å about a Ni atom in Ni metal at ~90 K.

TABLE I. Experimental phase-shift parameters for Ni-B, Ni-Ni, and Ge-Ge pairs [phase shift $\Phi(k)=P_0+P_1k+P_2k^2+P_3/k^3$].

Atom pair P-Q	Model system	$r_{P\text{-}Q}$ (Å)	P_0	P_1	P_2	P_3	Remarks
(1) Ni-B	Ni_2B crystal, 1–2 Å	2.14	0.8700	−1.6838	0.0624	8.16	Use values of Lee *et al.* (Ref. 46) as inputs
(2) Ni-Ni	Ni metal, 1–2.8 Å	2.492	1.1415	−1.1960	0.0284	−121.98	Same
(3) Ni-Ni	Ni_2B crystal, 2–3 Å	2.37	6.1434	−1.1934	0.0386	−348.92	Use outputs of (2) as inputs
		2.42	1.9470	−1.1714	0.0229	−439.76	
		2.70	0.9224	−1.1868	0.0299	−71.31	
		2.63	0.9687	−1.2112	0.0227	−281.73	
(4) Ni-B	Ni_2B crystal, 1–3 Å	2.14	1.0441	−1.6979	0.0617	−4.72	Used outputs of (1) and (3) as inputs
Ni-Ni		2.37	6.2060	−1.1910	0.039	−417.99	
		2.42	1.9980	−1.1660	0.0240	−504.57	
		2.70	0.9158	−1.1839	0.0300	−814.05	
		2.63	0.9564	−1.1897	0.0266	−333.96	
(5) Ge-Ge	Crystal Ge, 1–3 Å	2.45	3.5012	−1.1958	0.0275	−122.67	Use values of Lee *et al.* (Ref. 46) as inputs

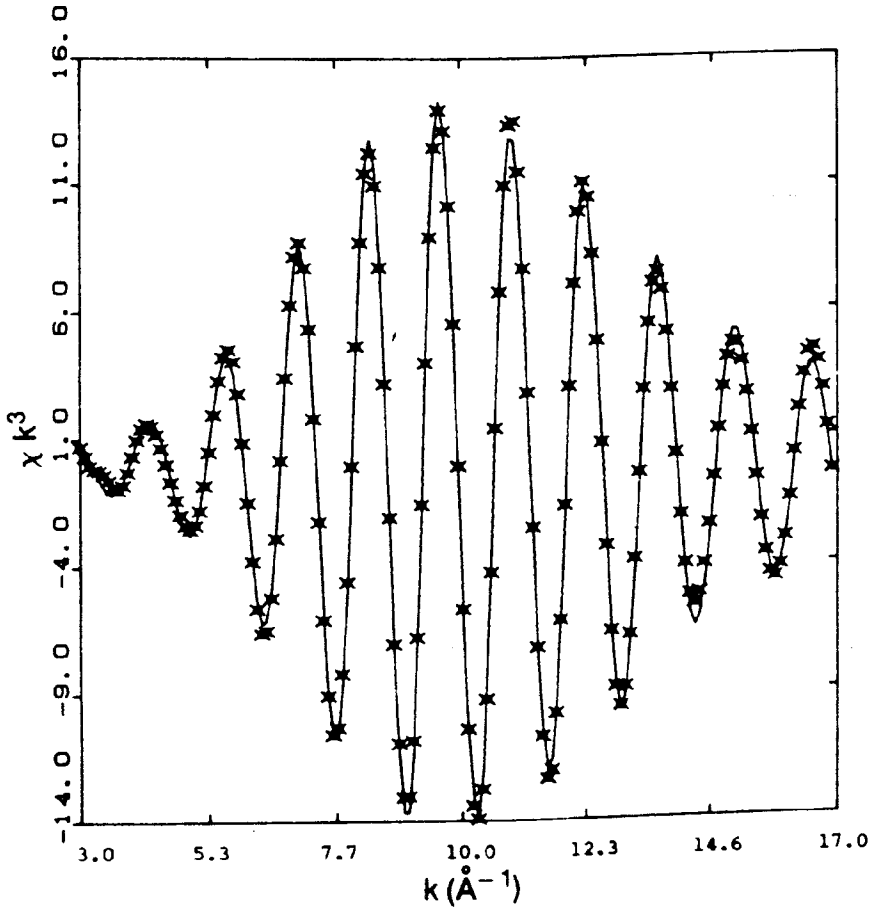

FIG. 9. Experimental (line) and simulated (points) EXAFS of the four Ni subshells in the region 2–3 Å about the central absorbing Ni atom in crystalline Ni_2B at ~90 K.

This generated a set of self-consistent experimental phase-shift parameters for the four Ni subshells in Ni_2B crystal. In this simulation, the same experimental Ni envelope function from the first shell of pure Ni, the Ni-Ni coordination numbers (1,2,4,4), and their bond distances (2.37, 2.42, 2.70, and 2.63 Å, respectively) in crystalline Ni_2B, $\Delta E_0=0$, and $\sigma^2=0$ were used as fixed inputs. The phase parameters P_i for each shell were allowed to vary. The simulation was made in χk^3 space and constituted a four-shell fitting. The results shown in Fig. 9 had a standard deviation of 2.7% of the maximum amplitude of the experimental $\chi^F k^3$. The derived Ni-Ni phase parameters are also given in Table I.

As can be seen, the phase shift derived empirically for the first Ni shell in pure fcc Ni metal at 2.492 Å was not strictly transferrable to any of the Ni-Ni shells in crystalline Ni_2B having a spread of distances from 2.37 to 2.70 Å. Such phase shift dependence on the distance between the center and backscattering atoms is a consequence of the breakdown of the small-atom approximation, first pointed out by Lee and Pendry[47] and latter emphasized by Pettifer.[48] The situation was studied in more detail by Bunker and Stern[49] in their phase analysis of a well-chosen series of tetrahedrally coordinated crystals Ge, GaAs, ZnSe, and CuBr.

3. *Combined determination of Ni-B and Ni-Ni phase shifts*

Having obtained the phase shift parameters separately for the Ni-B shell in Sec. IV B 1 and those for the four Ni-Ni shells in Sec. IV B 2, these phase-shift parameters were further fine-tuned in a combined five-shell fit on the filtered transform given in Fig. 2(f). This combined the EXAFS contributions of 4 B and 11 Ni neighbors about a central Ni atoms in the region 1–3 Å of the Fourier transform [Fig. 2(c)] for crystalline Ni_2B. The phase-shift parameters obtained from Secs. IV B 1 and IV B 2 were used as initial inputs for the Ni-B and Ni-Ni shells. N_j, r_j, σ_j^2, and E_0 identical to those in Secs. IV B 1 and IV B 2 were again used as fixed inputs. The simulation was made in χk^3 space. The results are shown in Fig. 10 and had a standard deviation of 4% of the maximum amplitude of the experimental $\chi^F k^3$ spectrum. The final phase shift parameters for Ni-B and Ni-Ni shells are given in Table I. It is noted that each set of final phase shift parameters varies little from the corresponding set obtained separately in Secs. IV B 1 and IV B 2. The combined fit and the fine-tuning was necessary since both the Ni-B and

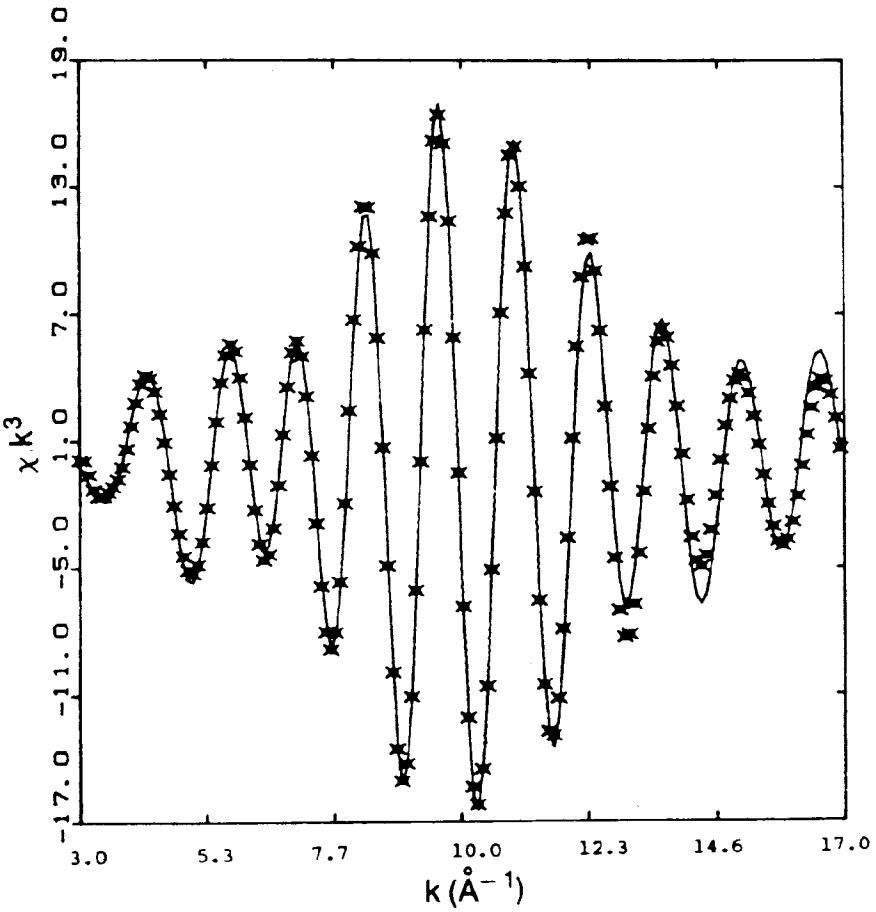

FIG. 10. Experimental (line) and simulated (points) EXAFS combining contributions from one B and four Ni subshells in the region 1–3 Å about the central absorbing Ni atom in crystalline Ni_2B at ~90 K

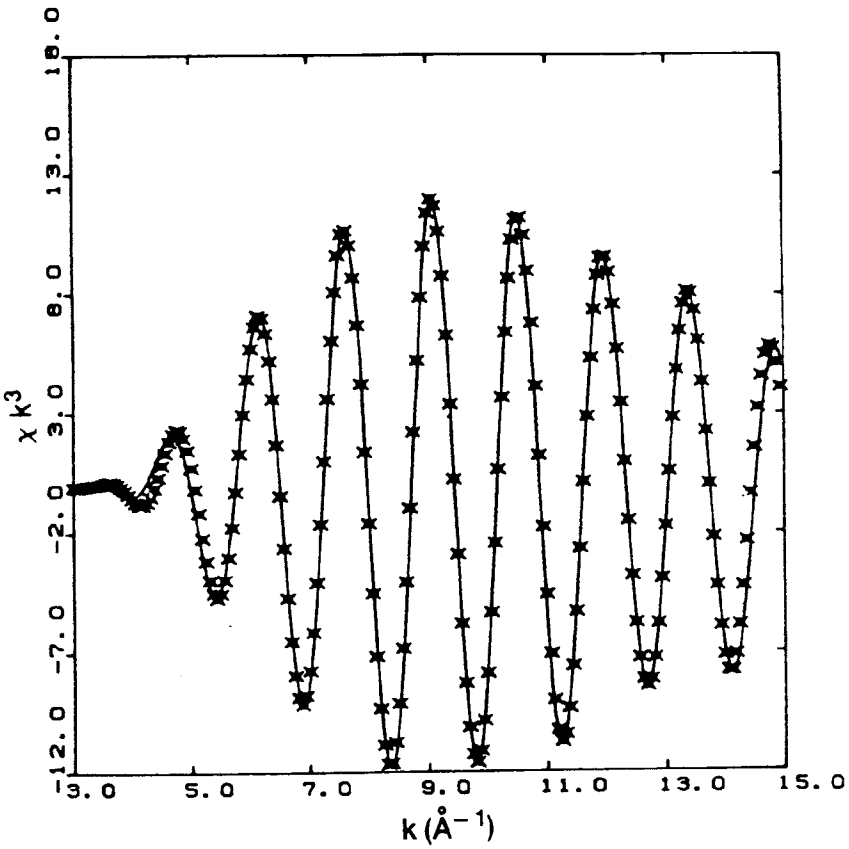

FIG. 11. Experimental (line) and simulated (points) EXAFS of the first shell of four neighbors in the region 1–3 Å about a central Ge in pure Ge at room temperature.

Ni-Ni shells in the structurally unknown glassy $Ni_{66}B_{33}$ had to be simulated simultaneously for the filtered EXAFS from one broad radial structure peak in the same region of real space 1–3 Å [see Figs. 1(c) and 1(d)].

4. *Determination of Ge-Ge phase shift and Ge envelope function*

The phase and envelope function for the Ge-Ge pair were generated in a similar manner by a self-fitting of the filtered EXAFS [Fig. 5(d)] signal from the first shell in pure Ge in the region 1–3 Å [Fig. 5(c)]. $N=4$, $r=2.450$ Å, $\Delta E_0=0$, and $\sigma^2=0$ were used as fixed parameters. The fitting was performed in χk^3 space. The results shown in Fig. 11 have a standard deviation of 4.5% of the maximum amplitude of the experimental $\chi^F k^3$. The Ge-Ge phase-shift parameters so obtained (Table I) were then used as fixed inputs to simulate the metalloid environment in Ge-substituted $Ni_{66}B_{15}Ge_{18}$ glass (see Sec. IV E).

C. Ni environment in $Ni_{66}B_{33}$ glass

The phase shifts and envelope functions for the Ni-B and Ni-Ni pairs extracted from the filtered experimental EXAFS of crystalline Ni_2B and fcc Ni metal as described above were then transferred and used to determine N, r, and σ^2 for the Ni atom in glassy $Ni_{66}B_{33}$. The σ^2 values for the glass were then calculated relative to the crystal values for the corresponding backscatterers (taken as zero as stated in Secs. IV B 1 and IV B 2 above). Curve fitting was performed systematically using various combinations of Ni-B and Ni-Ni subshells: 1 B + 1 Ni, 1 B + 2 Ni, 1 B + 3 Ni, 1 B + 4 Ni, 2 B + 1 Ni, and 2 B + 2 Ni. The number in these combinations denote the number of subshells (distinct interatomic distances). It was found that the 1 B + 3 Ni combination yielded the best fit with physically meaningful parameters for the glass. The results are shown in Fig. 12 and summarized in Table II.

It is seen that the number and distance of nearest boron atoms about a Ni constituent in the glass remain very similar to those of the crystal. This is not surprising since the metal-metalloid environment is expected to be largely determined by local chemical interactions, which in this case of nickel-boron, involves significant overlap of the boron p orbitals with the d orbital of the Ni.[50] Such local electronic interactions between chemically dissimilar pairs of constituent atoms are unlikely to differ in going from the crystal to the glassy phase of the same composition.

However, there is considerable rearrangement of the outer Ni shells about the central Ni atom. In the glass the

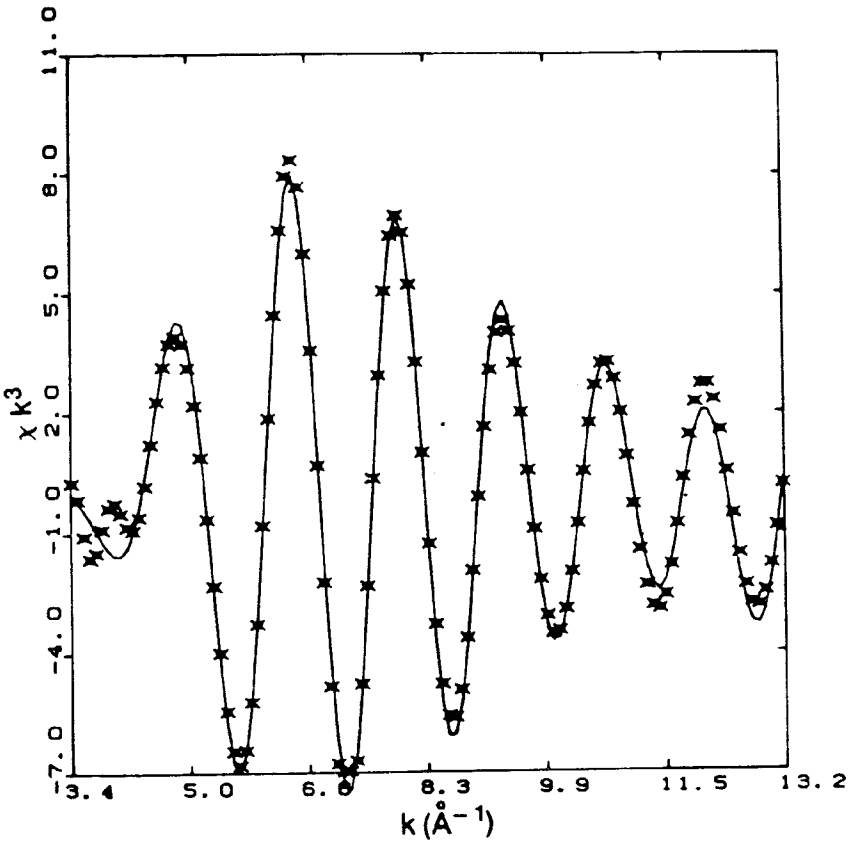

FIG. 12. Experimental (line) and simulated (points) EXAFS for $Ni_{66}B_{33}$ glass in the region 1—3 Å about the central absorbing Ni at ~90 K. The simulation was done using a combination of 1 B + 3 Ni subshells as described in the text.

11 Ni atoms are now distributed into three subshells with an ensemble average of 4, 3, and 4 atoms at 2.24, 2.46, and 2.63 Å, respectively. The shortest Ni-Ni distance in the glass is measurably shorter than that in the crystal at 2.37 Å (Table II). This local rearrangement and closer packing of the Ni subshells are indeed reflected in the overall local electronic structure of the glassy phase and manifested in changes of the near-edge spectral features, the so-called XANES (x-ray absorption near-edge structure) in going from the crystal to the glassy state.

TABLE II. Bond distances (r) and Ni coordination C_{Ni} in glassy and crystalline Ni_2B: Ni as central atom.

Glass		Crystal[c]	
C_{Ni}[a]	r (Å)[b]	C_{Ni}	r (Å)
3.8 B	2.11±0.03	4 B	2.14
4.3 Ni	2.24±0.09	1 Ni	2.37
3.0 Ni	2.46±0.06	2 Ni	2.42
		4 Ni	2.70
3.9 Ni	2.63±0.12	4 Ni	2.63
3.8 B + 11.2 Ni		4 B + 11 Ni	

[a]±10% or better.
[b]Spread in r value caluclated from σ_s^2 for the glass in Table III.
[c]Data from Ref. 24.

In Fig. 13(a) the normalized Ni K-edge XANES spectra for crystalline and glassy Ni_2B are plotted on the same scale in the range ±60 eV. Each spectrum was normalized by subtracting the linearly fitted line for the pre-edge from all points in the region ±60 eV and dividing the difference by the edge jump S as described in Eq. (1). The number of spectral features in the vicinity of the edge can be seen more clearly in the derivative spectra shown in Fig. 13(b). In the crystal, four distinct peaks are observed in the derivative spectrum in the region 0—20 eV. The actual energies of these spectral features in the normalized edge spectra [Fig. 13(a)] are give by the corresponding zeros on the high-energy side of the peaks in the derivative spectrum. Thus, in the case of crystalline Ni_2B, the four peaks in the derivative spectrum correspond to spectral features at 1.5, 5.5, 15, and 19 eV. The feature at 1.5 eV corresponds to the dipole forbidden $1s \rightarrow 3d$ transition and is weak. The feature at 5.5 eV may be assigned to the $1s \rightarrow 4p$ transition which is dipole allowed. This assignment is based primarily on the atomic energy levels for Ni given by Moore.[51] The features at 15 and 19 eV are mos likely due to the multiple-scattering effects.[52] In the glass the onset of edge absorption is negatively shifted by ~1.3

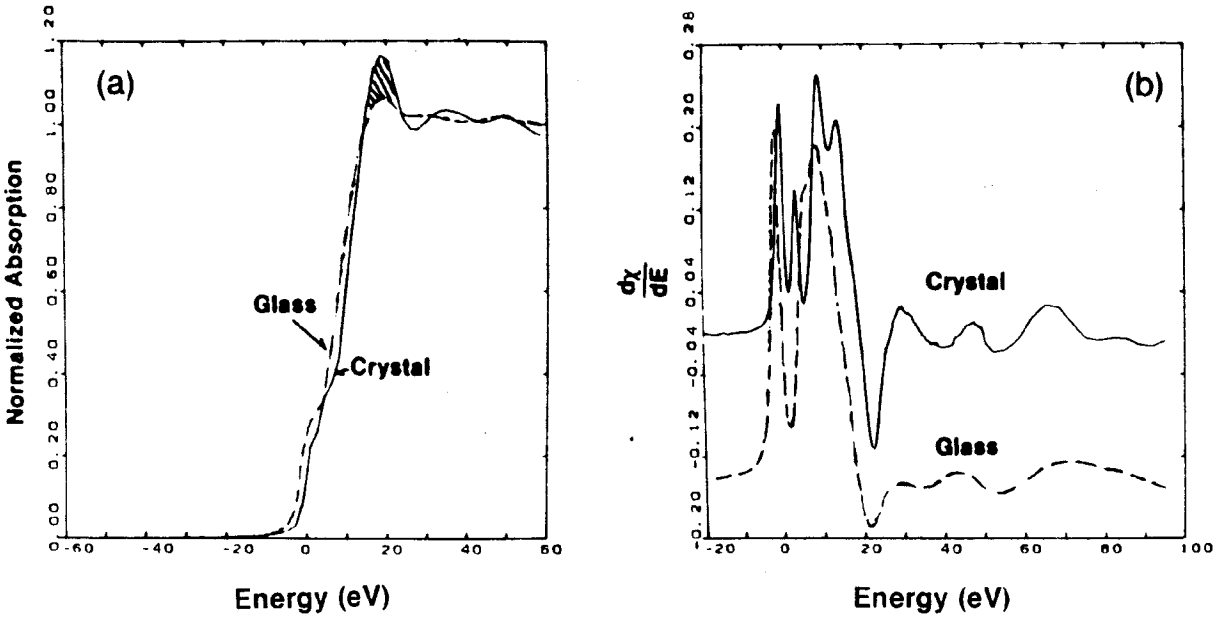

FIG. 13. (a) Normalized Ni K-edge XANES and (b) derivative spectra in crystalline and glassy Ni_2B at ~ 90 K. The various transitions in the range ± 20 eV can be seen more clearly in the derivative spectra. Features above 30 eV are EXAFS related.

eV with the respect to the crystal and the white line at 19 eV exhibits lower intensity. The negative shift may be due to an increase in the overlap of the Ni d orbitals as a result of a decrease in the shortest Ni-Ni distance of the innermost Ni subshell in the glass. However, the position of the $1s \rightarrow 3d$ transition remains approximately at ~ 1.5 eV. At higher energies the XANES spectrum is rather featureless. The derivative spectrum exhibit a broad peak in the same energy region where the crystal shows three well-defined peaks. This broad feature in the multiple-scattering regime merely reflects the existence of a distribution of Ni environments in the glass as compared with a unique c_{2v} site for Ni atoms in crystalline Ni_2B.

We now consider the Ni-Ni coordination geometry in the glass. From the EXAFS results, it is conceivable that the 11 Ni neighbors, on an ensemble average, are arranged in a slanting trigonal prism capped at all its five faces. In other words, the three subshells of Ni neighbors about a central Ni may be located as follows: The 3 Ni at 2.46 Å form an equilateral triangle containing the central Ni. The other two sets of 4 Ni at 2.24 Å and 2.63 Å form two penetrating (distorted) tetrahedra, each with an apex Ni lying along the C_3 axis of the trigonal prism. Indeed, a scaled stick model of $Ni\text{-}Ni_{11}$ cluster can be built with bond angles about the central Ni such that the three observed Ni-Ni distances can also be maintained between Ni atoms from any two subshells. This is depicted in Fig. 14. Furthermore, a rearrangement of the four Ni subshells in the crystal to three Ni subshells in the glassy may also be correlated with intensity redistribution of the white line in the XANES spectra shown in Fig. 13(a). This can be rationalized qualitatively since the electornic structure of a collection of particles (atoms) as well as multiple-

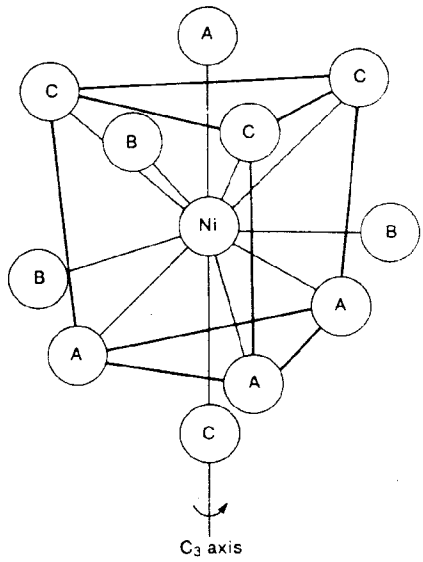

FIG. 14. Model of an average Ni coordination sphere about a central Ni atom in $Ni_{66}B_{33}$ glass. The 3 Ni at the B positions are at 2.46 Å, the 4 Ni at A are at 2.24 Å and the other four at C are at 2.63 Å. The overall cluster is a slanting (nonequal top and bottom triangles) and/or twisted (noneclipsing of A and C positions) trigonal prism with all its faces capping and having a C_3 symmetry.

scattering effects are a function of its atomic configuration.

Now we shall briefly discuss the results of fitting with other combinations of boron and nickel subshells. With 1 B + 1 Ni combination, nonphysical parameters such as negative σ^2 and $r_{\text{Ni-Ni}}$ values, small $N_{\text{Ni-Ni}}$ (<2) and/or large $N_{\text{Ni-B}}$ (8–11) resulted. In particular, it is worth noting that using an average Ni-Ni distance with a Debye-Waller width to approximate the local Ni-Ni correlation which has well-defined subshells with EXAFS distinguishable distances does *not* properly simulate the experimental EXAFS spectrum. This fact is borne out in crystalline Ni_2B which we used to model our EXAFS analysis for the glass. The four crystallographic Ni-Ni distances in the range 2.37–2.70 Å exhibit only a single radial structure peak in the region 2.3 Å in the Fourier transform of the EXAFS signal [Fig. 2(c)]. The present study can also serve to illustrate the power of the EXAFS technique over conventional diffraction in elucidating subshell structure in amorphous materials like metallic glasses. In an EXAFS event each distinguishable distance ($\Delta r \simeq 0.05$ Å) gives rise to a frequency, which has to be account for in order to simulate the experimental spectrum. Recently, Sadoc *et al.*[53] reported EXAFS studies on two well chosen metal-metal glass systems $Ni_{66}Y_{33}$ and $Cu_{60}Zr_{40}$ and successfully modeled the experimental pair distribution function about each constituent atom with two subshells of like-like and like-unlike pairs.

The fit was substantially improved within a range of meaningful N, r, and σ^2 parameters with the 1 B + 2 Ni subshells combination. For the Ni-B subshell, $N=4.57$, $r=2.11$ Å, and $\sigma^2=0.006$ Å^2. For the first Ni-Ni subshell, $N=5.12$, $r=2.25$ Å, and $\sigma^2=0.0073$ Å^2, and for the second Ni-Ni subshell, $N=2.69$, $r=2.45$ Å, and $\sigma^2=0.0029$ Å^2. The standard deviation of fit was 8% of the maximum value in χk^3 space. Compared with the crystal, the total number of Ni-Ni neighbors was still short by ~three atoms. Addition of the third Ni-Ni subshell with the 1 B + 3 Ni combination yielded further improvement to the fit and accounted for all 11 Ni atoms about a central Ni atom in the glass (Table II).

The 1 B + 4 Ni subshells combination was simulated in two ways: (a) by adding a fourth Ni-Ni subshell to the best fit of the 1 B + 3 Ni combination, and (b) by using the N_j and r_j values of crystalline Ni_2B as fixed inputs. For (a), nonphysical parameters for the fourth Ni-Ni subshell such as $N=48$, and $r=3.6$ Å (which was outside the range of the filtered experimental EXAFS) were obtained, indicating the unlikely possibility of a fourth Ni-Ni subshell within 3 Å of the Ni atoms in the glass. For the

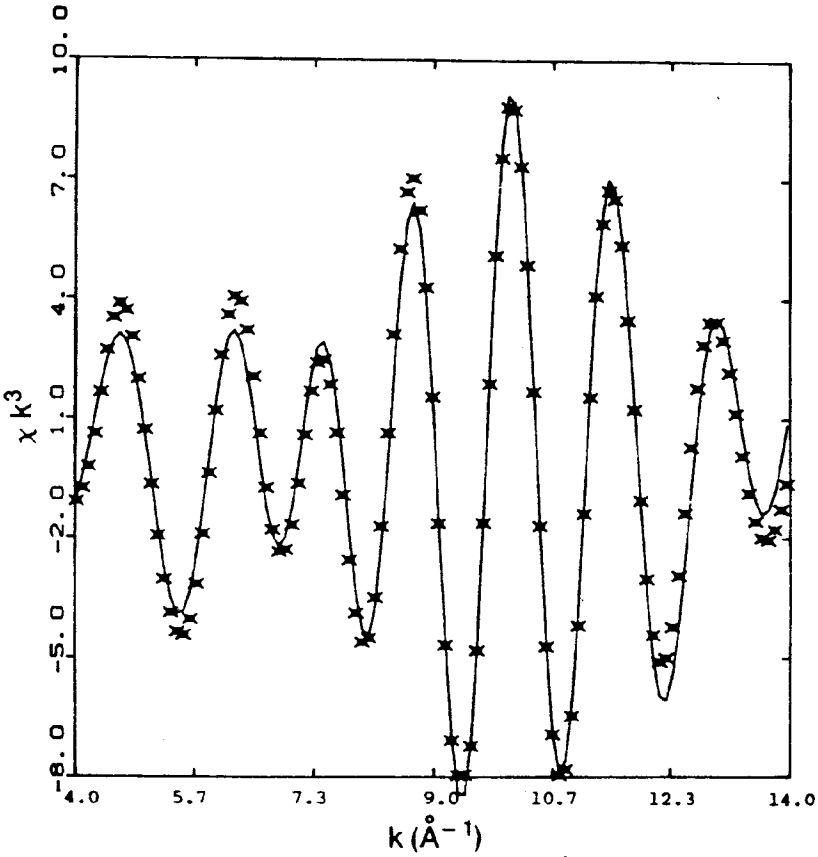

FIG. 15. Experimental (line) and simulated (points) EXAFS in the region 1–3 Å about the central absorbing Ni atom in crystalline Ni_2B at room temperature. The simulation was done merely by fitting the σ^2 value for each subshell with the corresponding structural parameters and same phase shift parameters derived for the same material at ~90 K (see Fig. 10).

case of (b), fixing either N_j or r_j produced nonphysical values for the other two structure parameters in the simulation. When both crystalline N_j and r_j values were used as fixed parameters and σ_j^2 allowed to vary, no convergent solution was possible. The simulated spectrum was totally incompatible with the experimental spectrum. *This clearly indicates that the Ni environment in $Ni_{66}B_{33}$ glass is not a broadened version of that in the parent Ni_2B crystal.* Similarly, nonphysical structural parameters resulted with 2 B + 1 Ni and 2 B + 2 Ni combinations. These require no further elaboration.

The above systematic simulation lends credence to the existence of subshell structure about the metal constituent in the $Ni_{66}B_{33}$ glass, as well as metal-metal glasses investigated by Sadoc *et al.*[53] The notion that short-range order in metallic glass is similar to or a broadened version of some parent crystal requires reexamination and qualification. In metal-metalloid glasses, similarity in the local structure is expected to persist in the metal-metalloid subshell since this is largely determined by the chemical interaction between the metal and metalloid atoms. The metal-metal distribution in the glass may vary to yield different subshell structure as seen in the present case of $Ni_{66}B_{33}$ glass. Thus, structural similarity between glass and crystal based primarily on peak positions in radial distribution functions from diffraction [30] and EXAFS[54] experiments cannot be fully substantiated.

D. Temperature effects

In simulating the low-temperature EXAFS spectra for the glass, the Debye-Waller factor for each subshell was evaluated with respect to the corresponding subshells in the crystal, the σ_j^2 of which were taken as zero. The σ_j^2 values so obtained were then a measure of the structural disorder of the glass with respect to the crystal at low temperature. These in turn yielded the spread of r_j values given in Table II for the glass. The thermal disorder for both the crystal and glass can now be determined by fitting the 300-K filtered-EXAFS spectra with the corresponding N_j and r_j values as fixed inputs and varying σ_j^2 only for each subshell. The results are shown in Figs. 15 and 16 and summarized in Table III. The fittings were 5% and 6% of the maximum value in χk^3 space for the crystal and glass, respectively.

For the glass, since the structural disorder is given by $\sigma_{90\,K}^2$ (by definition, relative to the crystal) the difference $\sigma_{300\,K}^2 - \sigma_{90\,K}^2$ yields the thermal disorder at 300 K. These

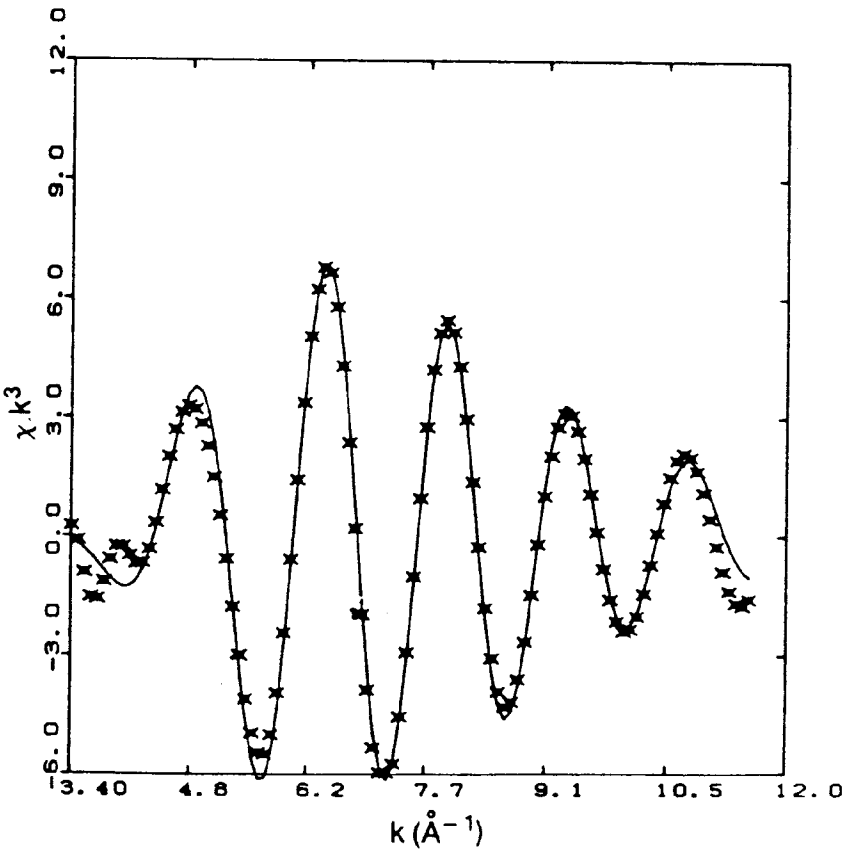

FIG. 16. Experimental (line) and simulated (points) in the region 1–3 Å about the central absorbing Ni in $Ni_{66}B_{33}$ glass at room temperature. The simulation was done merely by fitting the σ^2 value for each subshell with the corresponding structural parameters derived for the glass at ~90 K (see Fig. 11).

TABLE III. Structural σ_s^2 and thermal σ_{th}^2 disorder for various subshells in glassy $Ni_{66}B_{33}$ measured relative to those of crystalline Ni_2B taken as zero at ~90 K. Ni as central atom (σ^2 in Å^2).

Ni_2B crystal		$Ni_{66}B_{33}$ glass			
Subshell	$\sigma^2_{300\,K}$ ($=\sigma^2_{th}$)	Subshell	$\sigma^2_{90\,K}=\sigma^2_s$	$\sigma^2_{300\,K}$	$\sigma^2_{th}=\sigma^2_{300\,K}-\sigma^2_{90\,K}$
4 B at 2.14 Å	0.0021	3.8 B at 2.11 Å	0.0011[a]	0.0027	0.0016
1 Ni at 2.37 Å	0.0027	4.3 Ni at 2.24 Å	0.0083	0.0107	0.0024
2 Ni at 2.42 Å	0.0016	3.0 Ni at 2.46 Å	0.0035	0.0053	0.0018
4 Ni at 2.70 Å	0.0042				
4 Ni at 2.63 Å	0.0039	3.9 Ni at 2.63 Å	0.014	0.0204	0.006

[a]These values give the spread of bond distance for the glass in Table II.

values are comparable to those for the crystals with some differences. The thermal disorder for the Ni-B and shortest Ni-Ni subshells in the glass are slightly less than those of the crystals. This suggests stronger binding[55] of these two subshells in the glass in accordance with a decrease in interatomic distances found in the glass. It is interesting to note that the Ni-B distance in $Ni_{81}B_{19}$ glass was also determined to be 2.11 Å in a recent detailed and careful neutron scattering study by Lamparter *et al.*[19] The outer two Ni-Ni subshells in the glass exhibit higher thermal disorder compared with similar subshells in the crystal.

E. Metalloid environment in $Ni_{66}B_{33}$ glass

The Fourier-filtered Ge EXAFS from $Ni_{66}B_{15}Ge_{18}$ glass [Fig. 3(d)] was used to probe the metalloid environment in this glass. The simulation was done initially using one Ni shell. The Ni envelope function from Ni metal obtained in Sec. IV B 2 above and the theoretical phase shifts for[43] the Ge-Ni pair were used as fixed inputs. ΔE_0 was allowed to vary to redefine the k scale. N, r, and σ^2 were then iteratively evaluated. The fitting was performed in χk^3 space. The results shown in Fig. 17 have a standard deviation of 4.5% of the maximum magnitude of the ex-

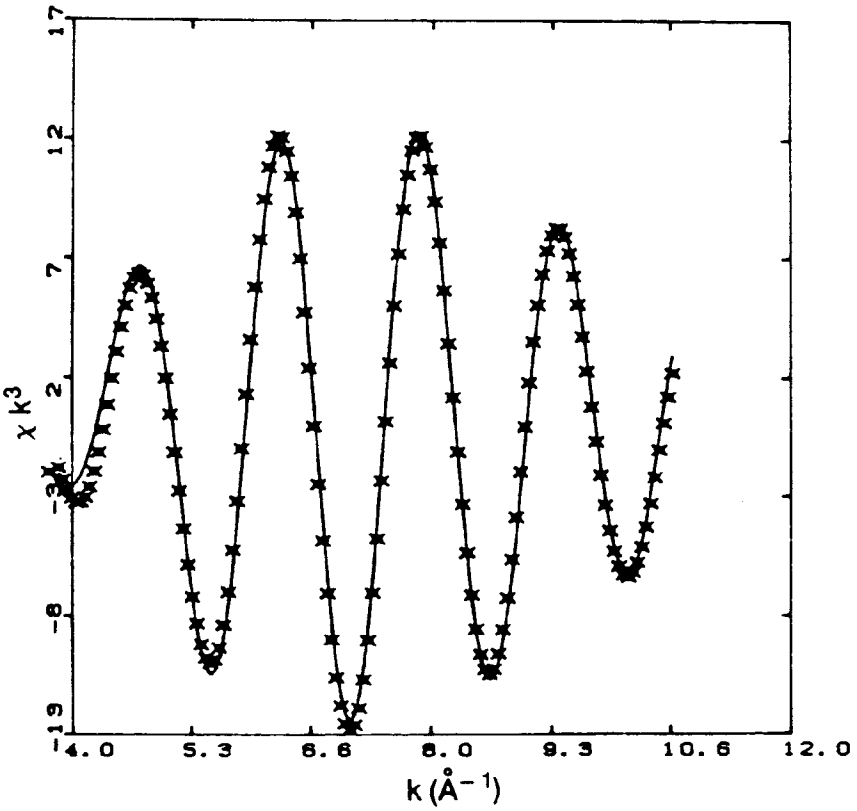

FIG. 17. Experimental (line) and simulated (points) EXAFS in the region 0.5–2.8 Å about the central absorbing Ge atom in glassy $Ni_{66}B_{15}Ge_{18}$ at ~90 K.

TABLE IV. Bond distance (r) and Ge coordination (C_{Ge}) in Ni-B-Ge and Ni-Ge glasses within a region of 3 Å.

System	C_{Ge}	r (Å)	σ^2 (Å^2)	Remark
$Ni_{66}B_{15}Ge_{18}$[a]	9.2 Ni[b]	2.37	0.0073	No detectable Ge-Ge contact neighbor
$Ni_{55}Ge_{45}$	4.0 Ni	2.31		Oyanagi *et al.* (Ref. 56)
	3.8 Ge	2.43		

[a] $\Delta E_0 = -3.2$ eV was fitted in using the theoretical phase shifts for the Ge-Ni pair.
[b] $= \pm 10\%$ or better.

perimental $\chi^F k^3$ spectrum. The best fitted number of Ni neighbors, the Ge-Ni separation, and the associated σ^2 value are given in Table IV.

To test the existence of metalloid-metalloid nearest neighbors in this type of high metalloid-content metallic glass, a subshell of Ge was added to simulate the same experimental Fourier-filtered Ge EXAFS given in [Fig. 3(d)]. Ge envelope and Ge-Ge phase shifts obtained from pure Ge in Sec. IV B 4 were used as fixed inputs. It was found that addition of a Ge subshell yielded diverging solutions with nonphysical parameters such as negative coordination number, negative σ^2 and/or large r value for the Ge-Ge pair. These simulations indicated that Ge-Ge nearest neighbor in $Ni_{66}B_{15}Ge_{18}$ glass is not likely to occur.

Thus, the Ge EXAFS results indicate that in the $Ni_{66}B_{15}Ge_{18}$ glass Ge is ninefold coordinated by Ni and there is no Ge-Ge contact neighbor. Compared with the boron environment in crystalline Ni_2B discussed above, the coordination of the metalloid constituent in the crystal is *not* preserved in the glassy state. In fact, ^{11}B NMR measurements which probe directly the electric field gradient, and hence site symmetry of boron, showed clearly that the triply peaked spectrum characteristic of boron in uniaxial symmetry in crystalline Ni_2B was not observed in the corresponding $Ni_{66}B_{33}$ glass.[31] Instead, a spectrum characteristic of boron in nonunixial symmetry similar to that of Ni_3B crystal was observed. Agreement of our Ge data with the ^{11}B NMR data showed general validity of the Ge substitution as probe of metalloid environment.

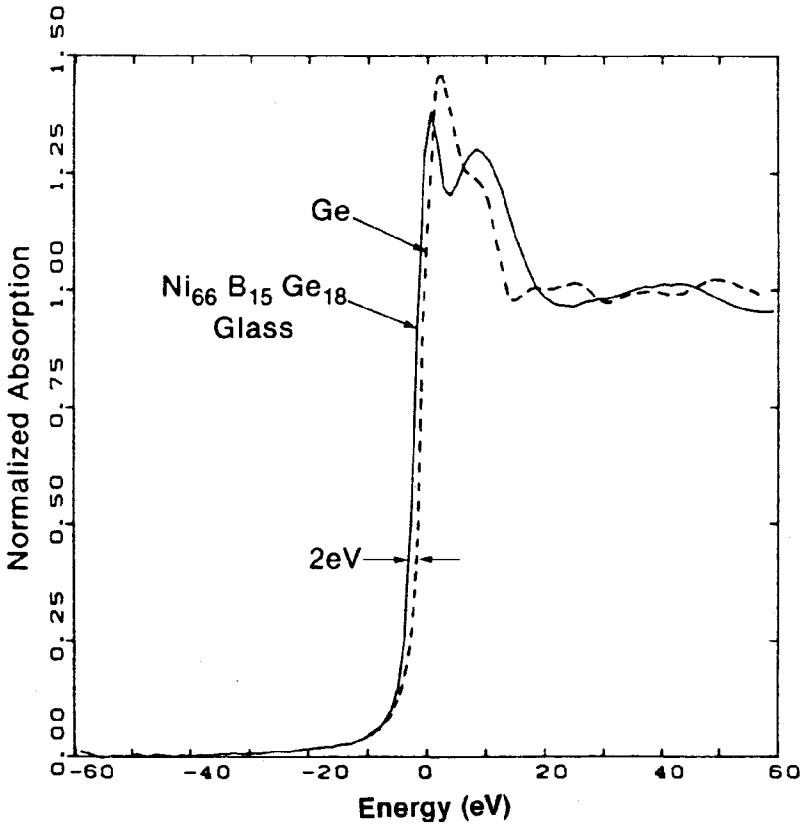

FIG. 18. Normalized Ge K-edge XANES spectra in crystalline Ge and $Ni_{66}B_{15}Ge_{18}$ glass at ~90 K.

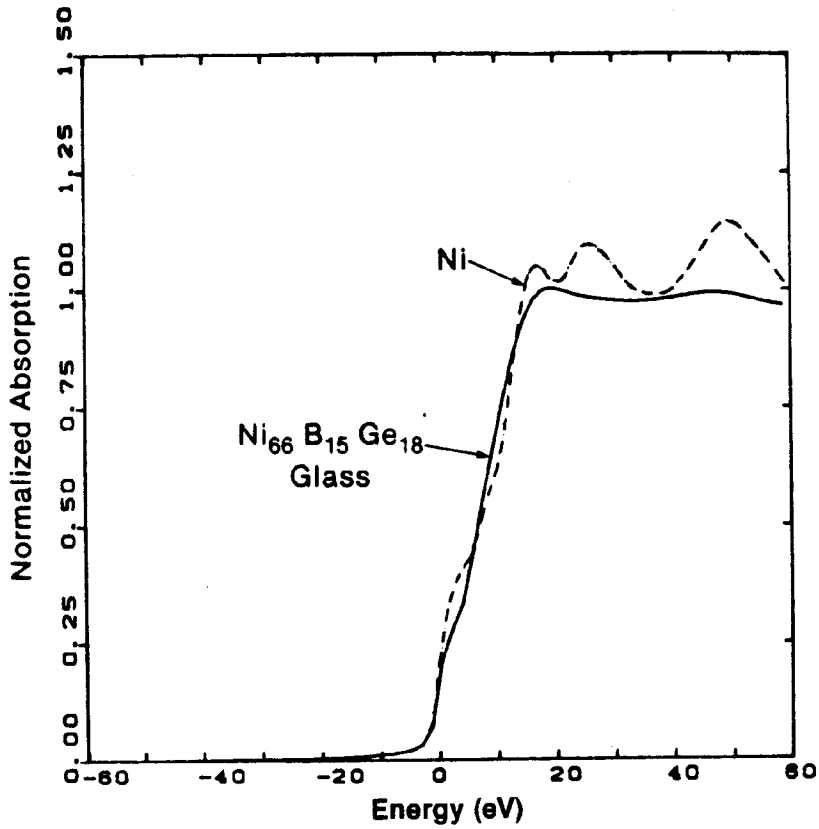

FIG. 19. Normalized Ni K-edge XANES in Ni metal and $Ni_{66}B_{15}Ge_{18}$ glass at ~90 K.

However, caution must be taken in deducing details of the boron environment from that of Ge since their electronic configurations and atomic radii are quite different. Of interest also is the Ge-Ni distance of 2.37 Å in the glass, which is much shorter than the sum of the Goldschmidt radii (1.25 Å + 1.37 Å = 2.62 Å), indicating that there is strong chemical interaction between Ni and Ge in the glass. The interaction can also be seen in the Ge K-edge white line in the XANES spectra for the glass and pure Ge shown in Fig. 18. This white line corresponds to a dipole-allowed transition from the $1s$ core to $4p$ final states, which are partially empty in the pure Ge solid, and its intensity is governed directly by the emptiness of the final p state. In the $Ni_{66}B_{15}G_{18}$ glass, when there exists electronic interaction between the metal and metalloid such that there is overlap of the Ni $3d$ with the Ge p states and vice versa, such overlap increases the occupancy (hence reduces the emptiness) of the Ge $4p$ states. This in turn reduces the probability of the $1s \rightarrow 4p$ transition and hence lowers its intensity as seen in Fig. 18. This electronic interaction is also manifested in the Ni K-edge XANES spectra shown in Fig. 19, which indicates an overall decrease in intensity of the XANES in the glass.

A similarly short Ge-Ni distance has been reported by Oyanagi *et al.*[56] on sputtered amorphous Ni-Ge films using a laboratory EXAFS apparatus. In all compositions investigated (7–55 at.% Ni), the Ge was found to coordinate both by Ni and Ge neighbors. At the composition $Ni_{33}Ge_{45}$, Ge is coordinated by 4.0 Ni at 2.31 Å and 3.8 Ge at 2.43 Å. The difference in Ge coordination between the sputtered and liquid-quenched materials may arise from differences between the two preparation methods as well as material composition. The sputtering route, which bypasses the liquid state, tends to yield a more randomized distribution of like and unlike pairs in a binary amorphous solid, whereas in splat quenching, liquidlike configurations are retained in the glassy solid as the system falls out of its internal equilibrium at the glass transition.

V. CONCLUDING REMARKS

The existence of Ni_2B in both the glassy and crystalline phases of known structure provided the experimental advantage of utilizing the EXAFS technique to gain insight into the metal environmental in metallic glasses. In crystalline Ni_2B, the Ni-Ni separations are distributed into four distinct distances or subshells, the EXAFS signal from which has been properly fitted using a multishell simulation with the single-scattering formalism. This simulation procedure produces a set of self-consistent Ni-Ni phase shift parameters which were transferred to simulate the coordination number and bond distances in tl glassy state from the experimental EXAFS signal. Systematic fitting indeed shows that a subshell structure of

Ni-Ni correlation, like that in the parent crystal, exists in the glass. However, the Ni neighbors are found to redistribute into three subshells with a measurably shorter Ni-Ni distance in the glass. This new finding has not been realized in previous EXAFS studies of metal-metalloid glass at the 80:20 composition, since there exists no appropriate crystal system to model the glass structure at the same composition.

Diffraction techniques have also been used extensively to study the pair distributions in the metallic glasses, particularly to distances beyond the first coordination sphere, and form a basis for testing various structural models. Perhaps the most detailed diffraction study of metal-metalloid glass is that by Lamparter *et al.*[19] in glassy $Ni_{81}B_{19}$ using an isotopic substitution for both Ni and B in their neutron scattering experiments. Nonetheless, the partial structure factor for the Ni-Ni pair yielded an overall coordination number with an average distance of separation. No subshell information was evident from the diffraction study.

Ge was used as an EXAFS probe for metalloid environment in $Ni_{66}B_{15}Ge_{18}$ glass since the B K edge is too low in energy to be measured at SSRL. Such substitution yielded informative results and can be shown to be generally valid when compared with ^{11}B NMR measurements of Ni-B glasses.[31] However, caution must be exercised when attempting to draw detailed conclusions about the boron environment from that of Ge since their atomic radii as well as electronic configurations are different. Finally, XANES spectra of constituent elements provide qualitative information on the chemical interactions between the metal and metalloid in the glass and complement structural data from the EXAFS region.

In summary, highlights of our EXAFS findings in this novel high metalloid content $Ni_{66}B_{33}$ glass as modeled by a multishell simulation with the corresponding Ni_2B crystal are the following.

(1) Around the central Ni atoms there exist both B and Ni "nearest" neighbors.

(2) The structure of the B coordination shell remains similar to that in the crystal in terms of the number of B neighbors about a central Ni atom and the Ni-B separation.

(3) As in the crystal, the Ni neighbors exist in subshells, but substantially rearranged and measurably closer to the central Ni atom. Neither the Ni-Ni distribution in the glass is a broadened version of that in the parent Ni_2B crystal nor the Ni-Ni separations can be described by an average value.

(4) In the Ge substituted $Ni_{66}B_{15}Ge_{18}$ glass, the Ge is coordinated only by Ni atoms (coordination number of ≈ 9). There is no Ge-Ge contact pair.

(5) The Ge-Ni distance is 2.37 Å, which is substantially shorter than the sum of their Goldschmidt radii of 2.62 Å, indicative of strong metal-metalloid interactions in the glass.

ACKNOWLEDGMENTS

We would like to thank F. W. Lytle for generously making available the EXAFIT program used in the present simulation study. His enlightening suggestions in the course of this work are much appreciated. Discussions with K. J. Rao and comments on the manuscript by R. P. Messmer, P. H. Gaskell, I. Bakonyi, and R. Frahm are also appreciated. We are also grateful for experimental opportunities at Stanford Synchrotron Radiation Laboratory (SSRL) supported by U. S. Department of Energy. One of us (J.W.) acknowledges partial support by the U. S. Department of Energy under contract No. DE-AC02-79ER-10382.

*Present address: Metglas Products—An Allied Chemicals Company, 6 Eastmans Road, Parsippany, NJ 07054.

[1]W. Klement, R. H. Willens, and P. Duwez, Nature (London) 187, 869 (1960).

[2]See chapters in *Amorphous Metallic Alloys*, edited by F. E. Luborsky (Butterworths, London, 1983).

[3]J. J. Gilman, Phys. Today 28 (5), 46 (1975).

[4]P. Chandhari and D. Turnbull, Science 199, 11 (1978).

[5]C. G. Grandquist and T. Claeson, Z. Phys. 20, 241 (1975).

[6]A. Calka, M. Madhara, D. E. Polk, B. C. Giessen, H. Matyja, and J. VanderSande, Scr. Metall. 11, 65 (1977).

[7]D. Turnbull, Contemp. Phys. 10, 473 (1969).

[8]R. C. Ruhl, B. C. Giessen, M. Cohen, and N. J. Grant, Acta. Metall. 15, 1693 (1967).

[9]T. W. Barbee, Jr., W. A. Holmes, D. L. Keith, and M. K. Pyzyma, Thin Solid Films 45, 591 (1977).

[10]S. Takayama, J. Mater. Sci. 11, 164 (1976).

[11]I. W. Donald and H. A. Davies, J. Non-Cryst. Solids 30, 72 (1978).

[12]D. E. Pole, Scr. Metall. 4, 117 (1970).

[13]J. D. Bernal, Nature (London) 185, 68 (1960); Proc. R. Soc. London Ser. A 280, 299 (1964).

[14]G. S. Cargill III, in *Solid State Physics*, edited by H. Ehrenreich, F. Seitz, and D. Turnbull (Academic, New York, 1975), Vol. 30, p. 227.

[15]T. M. Hayes, J. W. Allen, J. Tauc, B. C. Giessen, and J. J. Hausen, Phys. Rev. Lett. 40, 1282 (1978).

[16]S. R. Nagel, Scr. Metall. 12, 43 (1978).

[17]C. N. J. Wagner and H. Ruppersberg, At. Energy Rev. Suppl. 1, 101 (1981).

[18]J. Wong, in *Topics of Applied Physics*, edited by H. J. Güdtherodt and H. Beck (Springer, New York, 1981), Vol. 46, Chap. 4, pp. 45—77.

[19]P. Lamparter, W. Sperl, and S. Steeb, and J. Bletry, Z. Naturforsch 37A, 1223 (1982).

[20]H. S. Chen, T. Fugiwara, and Y. Waseda, J. Mater. Sci. 17, 1337 (1982).

[21]A. Inoue, A. Kitamura, and T. Masumoto, Trans. Jpn. Inst. Met. 20, 404 (1979).

[22]R. Ray, B. C. Giessen, and N. J. Grant, Scr. Metall. 2, 357 (1968).

[23]H. H. Liebermann and J. Wong, J. Non-Cryst. Solids 45, 195 (1981).

[24]E. E. Havinga, H. Damsma, and P. Hokkeling, J. Less-

Common. Met. 27, 169 (1972).
[25]J. L. Walter, P. Rao, E. Koch, and S. F. Bartram, Metall. Trans. 8A, 1141 (1977).
[26]U. Herold and U. Koster, *Rapidly Quenched Metals III* (Chameleon, London, 1978), Vol. 1, p. 281.
[27]T. Kemeny, I. Vincze, B. Fogarasy, and S. Arajs, Phys. Rev. B 20, 476 (1979).
[28]M. Takahashi, M. Koshimura, and T. Abuzuka, Jpn. J. Appl. Phys. 20, 1821 (1981).
[29]G. S. Chadha, N. Cowlan, H. A. Davies, and I. W. Donald, J. Non-Cryst. Solids 44, 265 (1981).
[30]F. A. Kuhnast, F. Machizand, and J. Flechon, J. Phys. (Paris) Colloq. 41, C8-250 (1980).
[31]P. Panissod, I. Bakonyi, and R. Hasegawa, J. Magn. Magn. Mater. 31-34, 1523 (1983).
[32]H. H. Liebermann, Mater. Sci. Eng. 43, 203 (1980).
[33]J. A. Beardon and A. F. Burr, Rev. Mod. Phys. 39, 125 (1967).
[34]H. H. Leibermann and C. D. Graham, Jr., IEEE Trans. Magn. 12(b), 921 (1976).
[35]E. E. Havinga, Philips Research Laboratories, Eindhoven, The Netherlands (1973).
[36]J. A. Kirby, Manual for Data Collection Program (University of California, Berkeley, 1978) (unpublished).
[37]F. W. Lytle, D. E. Sayers, and E. A. Stern, Phys. Rev. B 11, 4825 (1975).
[38]E. A. Stern, D. E. Sayers, and F. W. Lytle, Phys. Rev. B 11, 4836 (1975).
[39]B. Lengeler and P. Eisenberger, Phys. Rev. B 21, 4507 (1980).
[40]P. A. Lee, P. H. Citrin, P. Eisenberger, and B. M. Kincaid, Rev. Mod. Phys. 53, 769 (1981).
[41]C. DeBoor, J. Approx. Theorem 1, 219 (1968).
[42]For a compilation of x-ray cross sections, see W. H. McMaster, N. Nerr del Grande, J. H. Mallett, and J. H. Hubbell, Lawrence Radiation Laboratory Report No. UCRL-50/74, Sec. 2 Rev., 1969 (unpublished).
[43]B. K. Teo and P. A. Lee, J. Am. Chem. Soc. 101, 2815 (1979).
[44]G. Hagg, Z. Phys. Chem. 12, 413 (1931).
[45]G. H. Via, J. H. Sinfeet, and F. W. Lytle, J. Chem. Phys. 71, 690 (1979).
[46]P. A. Lee, B. K. Teo, and A. L. Simons, J. Am. Chem. Soc. 99, 3856 (1977).
[47]P. A. Lee and J. B. Pendry, Phys. Rev. B 11, 2795 (1977).
[48]R. F. Pettifer, in Proceedings of the Fourth European Physical Society General Conference, 1979, Chap. 7, p. 522.
[49]B. A. Bunker and E. A. Stern, Phys. Rev. B 27, (1983).
[50]R. P. Messmer, Phys. Rev. B 23, 1616 (1981).
[51]C. E. Moore, *Atomic Energy Levels*, National Stand. Ref. Data. Ser. (U.S. GPO, Washington, D.C., 1971), Vol. II.
[52]P. J. Durham, J. B. Pendry, and C. H. Hodges, Solid State Commun. 38, 159 (1981).
[53]A. Sadoc, D. Raoux, P. Lagarde, and A. Fontaine, J. Non-Cryst. Solids 50, 331 (1982).
[54]F. Schmuckle, P. Lamparter, and S. Steeb, Z. Naturforsch. 37a, 572 (1982).
[55]J. Wong and F. W. Lytle, Non-Cryst. Solids 37, 273 (1980).
[56]H. Oyanagi, K. Tsuji, S. Hosoya, S. Minomura, and T. Fukamachi, J. Non-Cryst. Solids 35, 555 (1980).